Barhl2 maintains T cell factors as repressors and thereby switches off the Wnt/β-Catenin response driving Spemann organizer formation

Elena Sena, Nathalie Rocques, Caroline Borday, Harem Sabr Muhamad Amin, Karine Parain, David Sitbon, Albert Chesneau, Beatrice Claude Durand

© 2019. Published by The Company of Biologists Ltd | Development (2019) 146, dev173112. doi:10.1242/dev.173112

RESEARCH ARTICLE

Barhl2 maintains T cell factors as repressors and thereby switches off the Wnt/β-Catenin response driving Spemann organizer formation

Elena Sena[1,*], Nathalie Rocques[1,‡], Caroline Borday[1,3], Harem Sabr Muhamad Amin[2,§], Karine Parain[3], David Sitbon[4], Albert Chesneau[3] and Béatrice C. Durand[1,2,¶]

ABSTRACT

A hallmark of Wnt/β-Catenin signaling is the extreme diversity of its transcriptional response, which varies depending on the cell and developmental context. What controls this diversity is poorly understood. In all cases, the switch from transcriptional repression to activation depends on a nuclear increase in β-Catenin, which detaches the transcription factor T cell factor 7 like 1 (Tcf7l1) bound to Groucho (Gro) transcriptional co-repressors from its DNA-binding sites and transiently converts Tcf7/Lymphoid enhancer binding factor 1 (Lef1) into a transcriptional activator. One of the earliest and evolutionarily conserved functions of Wnt/β-Catenin signaling is the induction of the blastopore lip organizer. Here, we demonstrate that the evolutionarily conserved BarH-like homeobox-2 (Barhl2) protein stabilizes the Tcf7l1-Gro complex and maintains the repressed expression of Tcf target genes by a mechanism that depends on histone deacetylase 1 (Hdac-1) activity. In this way, Barhl2 switches off the Wnt/β-Catenin-dependent early transcriptional response, thereby limiting the formation of the organizer in time and/or space. This study reveals a novel nuclear inhibitory mechanism of Wnt/Tcf signaling that switches off organizer fate determination.

KEY WORDS: Organizer, Groucho/Tle, Tcf/Lef, Barhl2, Hdac, Stem cells, Wnt, Pluripotency, Transcription

INTRODUCTION

The Wnt/β-Catenin signaling pathway has many important roles in embryogenesis, stem cell biology and tumorigenesis (reviewed by Cadigan, 2012; Holland et al., 2013; Nusse and Clevers, 2017). The key step in the transcriptional activation mediated by the canonical Wnt pathway is the nuclear increase of β-Catenin levels that transiently converts T cell factors (Tcfs, also known as transcription factors)/Lymphoid enhancer binding factor 1 (Lef1), bound to Wnt-responsive enhancers (WREs) into a transcriptional activator (Behrens et al., 1996) (reviewed by Cadigan and Waterman, 2012; Clevers and Nusse, 2012). In the Wnt 'off' state, Tcfs interact with Groucho (Gro)/Transducin-like Enhancer-of-split (Tle) proteins and act as transcriptional repressors (Roose et al., 1998; Brantjes et al., 2001; Daniels and Weis, 2005) (reviewed by Cinnamon and Paroush, 2008; Jennings and Ish-Horowicz, 2008; Ramakrishnan et al., 2018). The net transcriptional readout of the canonical Wnt signaling pathway is dependent on both the cell and developmental context. Given that β-Catenin is the sole mediator of these Wnt transcriptional responses (Schuijers et al., 2014), the response diversity could be explained by either epigenetic mechanisms or developmental stage-specific Tcfs (Roël et al., 2002; Blythe et al., 2010; Hikasa et al., 2010) (reviewed by Sokol, 2011; Cadigan, 2012; Nakamura and Hoppler, 2017), both of which are poorly understood.

In vertebrate embryos, different Tcf isoforms have distinct activities (reviewed by Cadigan and Waterman, 2012). Some, such as Lef1 or Tcf7 (also known as Tcf1), are required for transcriptional activation (reviewed by Arce et al., 2006), whereas others, such as Tcf7-like 1 (Tcf7l1, also known as Tcf3) mostly act as transcriptional repressors (Houston et al., 2002; Liu et al., 2005). The Gro/Tle family of proteins is conserved in Metazoa. The Gro proteins do not have a DNA-binding domain and rely on their interaction with transcription factors for their specific recognition of promoter and/or enhancer DNA sequences (reviewed by Cinnamon and Paroush, 2008; Jennings and Ish-Horowicz, 2008). Gro proteins bind Tcfs via their glutamine-rich (Q) domain (Cadigan and Waterman, 2012). Gro proteins also contain a WD-repeat domain, which interacts with the Engrailed Homology 1 (EH1) motif. The EH1 motif mediates transcriptional repression *in vivo* and *in vitro* and is present in numerous homeodomain-containing transcription factors (Fig. S1) (Smith and Jaynes, 1996; Jimenez et al., 1997; Pickles et al., 2002) (reviewed by Copley, 2005). Both Tcf and Gro proteins interact with histone deacetylases (Hdacs), which establish regional repressive chromatin structures (Chen et al., 1999; Billin et al., 2000; Eshelman et al., 2017) (reviewed by Laugesen and Helin, 2014; Seto and Yoshida, 2014). Until now, there has been little information on developmental contexts in which Tcf and/or Gro proteins mediate transcriptional silencing via Hdac activity (Kaul et al., 2014; Chambers et al., 2017) (reviewed by Cinnamon and Paroush, 2008).

One of the earliest, well-documented and evolutionarily conserved functions of Wnt/β-Catenin signaling is the induction of the blastopore lip organizer (Kraus et al., 2016). In *Xenopus* embryos, before initiation of zygotic transcription (stage 7), maternal determinants stabilize β-Catenin on the dorsal side of the

[1]Institut Curie, Research Division, PSL Research University, Université Paris Sud, CNRS UMR 3347, INSERM U1021, Centre Universitaire, Bâtiment 110, Orsay Cedex F-91405, France. [2]Ecole Normale Supérieure, Institut de Biologie de l'ENS, IBENS, S1.7 CNRS 8197, INSERM U1024 46 rue d'Ulm 75005, Paris F-75005, France. [3]Paris-Saclay Institute of Neuroscience, CNRS, Université Paris Sud, Université Paris-Saclay, 91405 Orsay 91405, France. [4]Institut Curie, PSL Research University, CNRS, UMR3664, Equipe Labellisée Ligue contre le Cancer, Paris 75005, France.
*Present address: Department of Cell, Developmental and Regenerative Biology, Icahn School of Medicine at Mount Sinai, New York, NY 10029, USA. ‡Present address: Ecole Polytechnique, Université Paris-Saclay, CNRS UMR 7654, Palaiseau 91120, France. §Present address: Department of Biology, College of Science, University of Sulaimani, Sulaymaniyah 46001, Kurdistan Region, Iraq.

¶Author for correspondence (beatrice.durand@curie.fr; beatrice.durand@sorbonne-universite.fr)

E.S., 0000-0003-1220-5639; C.B., 0000-0001-8531-409X; D.S., 0000-0002-4131-8520; B.C.D., 0000-0002-0047-288X

Received 25 October 2018; Accepted 11 April 2019

Development (2019) 146, dev173112. doi:10.1242/dev.173112

embryo (Schneider et al., 1996; Larabell et al., 1997). At the same stage, maternally encoded Tcf7l1 represses gene transcription throughout the embryo (Houston et al., 2002). In the presumptive organizer territory, the local increase in nuclear β-Catenin derepresses Tcf7l1 and initiates the dorsal development program that leads to Spemann organizer formation (Molenaar et al., 1996; Schneider et al., 1996; Roose et al., 1998; Houston et al., 2002; Xanthos et al., 2002; Tao et al., 2005; Blythe et al., 2010). A genome-wide study performed in *Xenopus laevis* (*X. laevis*) identified all the genes derepressed by β-Catenin in the dorsal part of the embryo (Ding et al., 2017). After initiation of the zygotic program, a second wave of Wnt signaling, driven by *wnt family member 8a* (*wnt8a*) expressed in the ventrolateral mesoderm, promotes development of the posterior part of the embryo. Using both RNA-sequencing (seq) and chromatin immunoprecipitation (ChIP)-seq approaches, direct and indirect target genes of zygotic Wnt8a signaling have been identified (Kjolby and Harland, 2017; Nakamura and Hoppler, 2017). Comparing the early and late Wnt signatures revealed that all but three of the early dorsal β-Catenin target genes are unresponsive to the second wave of Wnt signaling (Ding et al., 2017).

We previously investigated the embryological roles of the transcription factor BarH-like homeobox 2 (Barhl2), which carries two EH1 motifs (reviewed in Schuhmacher et al., 2011; Juraver-Geslin and Durand, 2015; Sena et al., 2016). In *Xenopus* embryos, *barhl2* is expressed in the neural plate and the diencephalic primordium. Barhl2 promotes apoptosis in the neuroectoderm and mesoderm, thereby influencing the Bone morphogenetic protein (Bmp) and Sonic hedgehog (Shh) signaling activity gradients within the neural plate (Offner et al., 2005). On the basis of the patterns of apoptosis (Hensey and Gautier, 1998; Yeo and Gautier, 2003), we suggested that Barhl2 acts on the formation of the axial organizing center, that is, the prechordal plate and the notochord, which are two tissues derived from the Spemann organizer (Offner et al., 2005). We also demonstrated that, within the diencephalic primordium, Barhl2 limits β-Catenin transcriptional activation (Juraver-Geslin et al., 2011). RNA-seq databases report the presence of a small number of *barhl2* transcripts at stages 8.5-9, when the Spemann organizer forms (Owens et al., 2016; Session et al., 2016; Ding et al., 2017), but developmental apoptosis only occurs after the onset of gastrulation (Hensey and Gautier, 1997). Taken together, these observations suggested that Barhl2 influences the establishment of the Spemann organizer through its activity as a brake on Wnt/β-Catenin-mediated transcriptional activation.

In the present study, we investigated the molecular mechanisms by which Barhl2 influences the Wnt/β-Catenin transcriptional response, using *Xenopus* embryos and mammalian cells as model systems. We show that Barhl2 limits both the size and the signaling activity of the Spemann organizer and that overexpressed Barhl2 abolishes Spemann organizer formation. In both mammalian cells and *X. laevis*, Barhl2 directly binds to Gro4 via its EH1 motifs, and interacts with Tcf7l1 independently of Gro. Using Wnt/Tcf reporter activity assays *in vitro* and *in vivo*, we demonstrate that Barhl2 prevents the β-Catenin-induced Tcf transcriptional activation switch and inhibits both Tcf7l1, and Tcf7 to activate the early β-Catenin response, probably by interacting with them when bound on DNA. Our data also indicate that Barhl2 promotes Hdac1-dependent repression of Spemann organizer formation and deacetylation of key organizer gene promoters. Taken together, our observations demonstrate that Barhl2 switches off the first wave of Wnt/β-Catenin transcriptional activity, therefore limiting in time and/or space the Spemann organizer induction process.

RESULTS

In *Xenopus* embryos, Barhl2 participates in the establishment of the early organization plan

RNA-seq databases report a small peak of *barhl2* expression (4000 transcripts) between stages 7.5 and 9.5; expression drops to low levels at stage 10 and then rises again at stage 12.5, with an average number of 10^5 transcripts detected at stage 14 (Owens et al., 2016; Session et al., 2016). Using RT-quantitative PCR (RT-qPCR) on individual embryos, we confirmed the presence of *barhl2* transcripts in blastula embryos (Fig. 1A). Using whole-mount *in situ* hybridization (ISH), we observed *barhl2* transcripts in the presumptive organizer region at stage 8.5 (Fig. 1B). Using non-quantitative RT-PCR analysis on batches of embryos, we were previously unable to detect *barhl2* expression at stage 8 (Offner et al., 2005). This discrepancy probably reflects sensitivity differences in the RNA detection methods used.

We next assessed whether Barhl2 acts in the establishment of the anteroposterior (AP) and dorsoventral (DV) axis of *X. laevis* embryos. To deplete Barhl2 activity, we used previously characterized morpholinos (MOs) (Offner et al., 2005) (see Materials and Methods). MO depletion of Barhl2 activity generated an anteriorization phenotype, with stage-25 embryos exhibiting enlarged cement glands (Fig. 1Ca,b). Conversely, both mice (*mBarhl2*) and *Xenopus barhl2* (*xbarhl2*) mRNA injections generated ventralized embryos, lacking dorsoanterior structures (Fig. 1Cd,e). Injection of a *barhl2*-encoding DNA vector that requires zygotic transcription to be expressed (Christian and Moon, 1993) generated embryos with diminished dorsoanterior structures, particularly a diminished cement gland (Fig. 1Cf). For each condition, the penetrance of the phenotype was quantified (Fig. 1D). We previously established a specific dose-dependent inhibition of *barhl2* mRNA translation by *MObarhl2* (Offner et al., 2005). Here, we further confirmed that, at two different doses, injection of *Barhl2*, which does not carry a sequence complementary to that of *MObarhl2*, rescued the enlargement of the cement gland induced by depletion of endogenous Barhl2 activity (Fig. 1E).

Taken together, these findings provide evidence that *barhl2* transcripts are present in the presumptive organizer territory, and that Barhl2 normally helps establish the embryo organization plan.

Barhl2 limits Spemann organizer development and signaling

We next investigated the role of Barhl2 on Spemann organizer formation and signaling. We measured changes in *chordin* (*chd*) expression territory in stage-10 *barhl2* gain-of-function (GOF) and loss-of-function (LOF) embryos using a new ImageJ macro (see Materials and Methods). In both GOF and LOF conditions, we observed significant differences between the injected and control sides (Fig. 2AB; Fig. S2): Barhl2 overexpression decreased the *chd* expression territory, whereas Barhl2 depletion increased it (Fig. 2A,B).

Using RT-qPCR on individual stage 8-10 embryos depleted of Barhl2 activity, we quantified expression changes in both organizer genes [*barhl2*, *siamois1* (*sia1*), *chd*, *goosecoid homeobox* (*gsc*), *orthodenticle homeobox 2* (*otx2*) and *notochord homeobox* (*not*)] and ventro/lateral mesoderm markers [*vent homeobox 2* (*vent2*), *wnt8a* and *brachyury*] (Fig. 2C). In agreement with a role for Barhl2 after stage 8, we did not detect significant changes in the expression of *sia1*. However, we detected a 2-5-fold increase in the expression of all the organizer genes analyzed (Fig. 2C). By contrast, we found a decrease in all the ventro/lateral mesoderm markers analyzed (Fig. 2C). Using ISH on stage-10 embryos, we confirmed these observations on Barhl2-depleted embryos (Fig. S3). By contrast, stage-10 *xbarhl2*-overexpressing embryos exhibited a decrease in

Development (2019) 146, dev173112. doi:10.1242/dev.173112

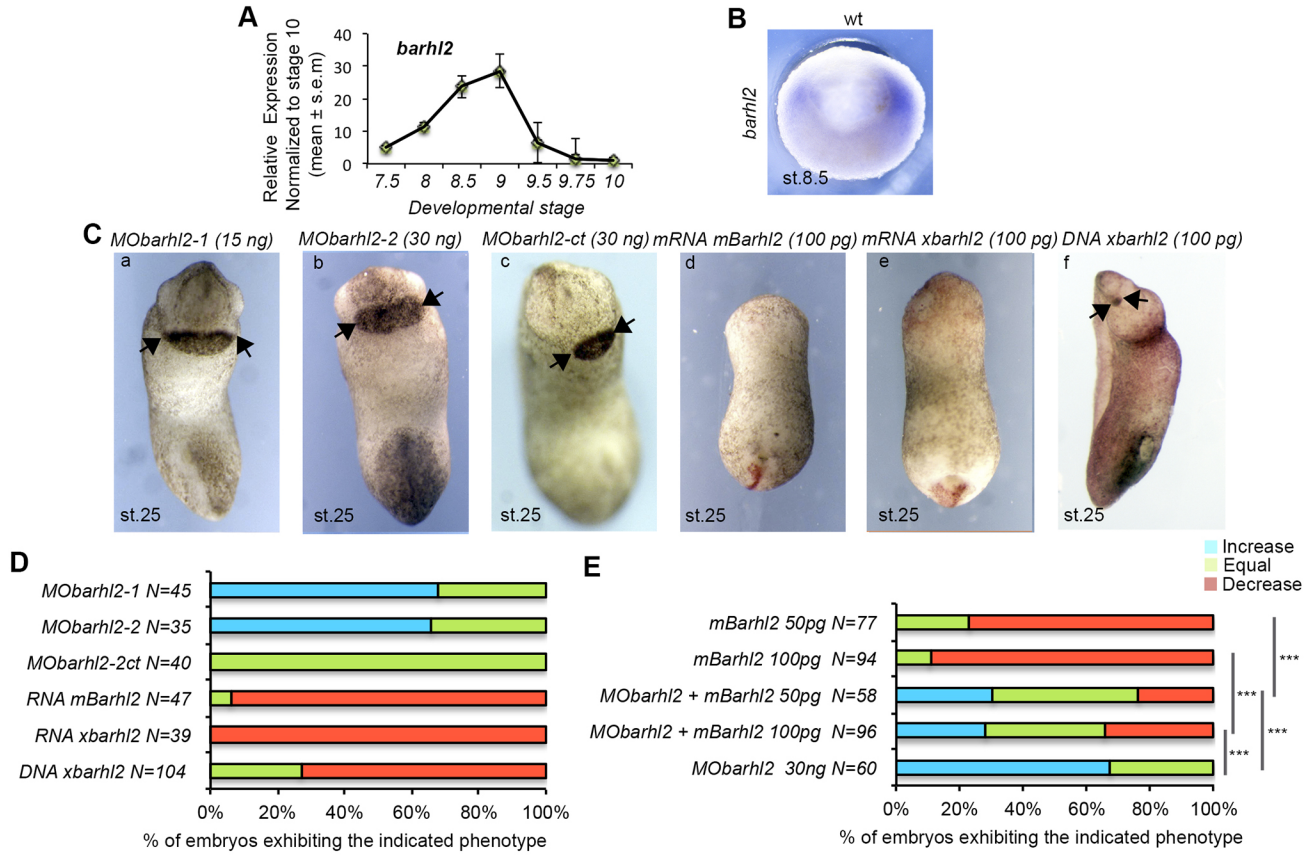

Fig. 1. Barhl2 influences the establishment of the organizational plan of the *Xenopus* neurula. (A) RT-qPCR for *Xenopus laevis barhl2* from at least 10 individual embryos stage (st)-7.5-10 embryos. Error bars correspond to biological replicates. (B) ISH using *xbarhl2* as probe showing expression in the presumptive organizer territory. A half-sliced embryo at st 8.5 is shown animal side up, dorsal right. (C) Representative st-25 embryos injected as indicated. The length of the cement gland (CG, black arrow) was measured using ImageJ. A CG of 1.2 times the average size of its wt siblings is considered increased. A CG of 0.8 times the average size of its wt siblings, or absent, was considered decreased. (D) Quantification of C. (E) Quantification graph showing that *Barhl2* rescues the *MObarhl2*-induced CG phenotype.

otx2 and *gsc* territories, and an increase in *wnt8a* and *vent2* territories (Fig. S3). Therefore, Barhl2 LOF increased the expression of key organizer genes, whereas Barhl2 GOF decreased it.

During gastrulation, the Spemann organizer and its derived structures, the prechordal plate and notochord, produce planar and vertical signals (including Bmp inhibitors and Shh) that induce and pattern the mesoderm and the emerging nervous system (reviewed in De Robertis and Kuroda, 2004; Niehrs, 2004; Stern, 2006). We tested whether Barhl2 acts on this organizer signaling activity and thereby also influences patterning of the neuroepithelium.

Our previous analysis of the effects of Barhl2 on early neurula phenotypes demonstrated that Barhl2 influences the Shh and Bmp signaling gradients within the neural plate (Offner et al., 2005; Juraver-Geslin et al., 2011). Here, we confirmed that Barhl2 depletion produced a widening of the neuroepithelium and associated defects in AP and DV patterning of the neural plate (Fig. S4A). We hypothesized that the impact of Barhl2 GOF and LOF on neuroepithelium patterning resulted from Barhl2 acting on Spemann organizer formation. However, to exclude the possibility that Barhl2, which is undetectable in the dorsal ectoderm, nonetheless acted by changing the response of these ectodermal cells to extracellular signals, we targeted Barhl2 depletion to different parts of the dorsal tissues of the embryo. Based on the expression of a co-injected tracer, we assessed retrospectively whether *MObarhl2* was injected in the dorsal mesoderm and axial dorsal ectoderm or in the lateral mesoderm and lateral ectoderm (Fig. 2Da). We observed the characteristic increase in *sry box 3* (*sox3*) territory only when Barhl2 depletion was targeted to the presumptive organizer territory that arises from the dorsal mesoderm (Fig. 2Db; Fig. S4B,C).

Thus, we conclude that Barhl2 normally limits the extent of the Spemann organizer territory and, consequently, the signaling activity of the organizer.

Barhl2 binds Gro4 and Tcf7l1 independently and prevents β-Catenin-driven derepression of Tcf synthetic target genes

We tested whether Barhl2 activity on organizer formation requires its DNA-binding domain, its EH1 domains, or both (Fig. 3A).

In full-length *barhl2* (*barhl2*fl), we mutated amino acids (AAs) in the homeodomain (HD) known to be instrumental for the correct binding to target DNA, to generate *barhl2flHoxM* (Fig. 3A) (Bürglin and Affolter, 2016). We also removed the EH1 motifs to generate *barhl2ΔEHs* and mutated three AAs in each EH1 motif to generate *barhl2flEHsM* (Fig. 3A). As discussed earlier, Barhl2 activity on the neural plate size is at least partly an indirect consequence of its activity on the Spemann organizer. At stage 14, Barhl2 GOF caused a decrease in the size of the neural plate (Fig. 3Ba,C) (Offner et al., 2005). By contrast, overexpression of mutant forms of *barhl2* cDNA did not affect the size of the neural plate nor the expression of organizer and ventro/lateral mesoderm markers (Fig. 3Bb-d,C; Fig. S5). Therefore, Barhl2 activity on

Development (2019) 146, dev173112. doi:10.1242/dev.173112

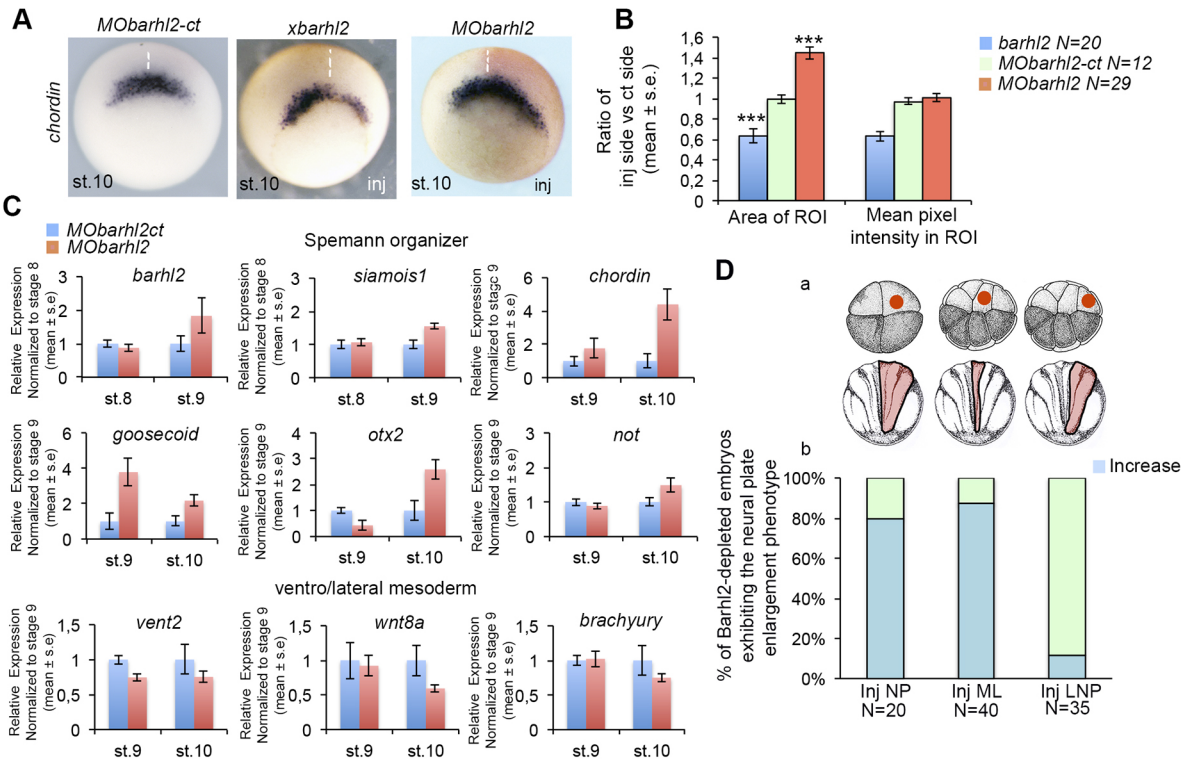

Fig. 2. Barhl2 limits the extension and signaling of the Spemann organizer. (A) ISH on stage (st) 10 embryos injected (inj) as indicated using *chd* as a probe. (B) Quantification of ROI area and mean pixel intensity in ROI on embryos from A. (C) RT-qPCR on RNA extracted from st 8-10 embryos on Spemann organizer and ventro/lateral mesoderm genes. For each experiment (*n*=2), five individual embryos were lysed. (D) (a) Scheme of the experiment: embryos were injected into one dorsal blastomere at the 4- or 16-cell stage with *MObarhl2* and a tracer. Dorsal view of a st-14 injected embryo showing the site of injection (red dot), and the targeted territory (in red); (b) quantification of the experiment in a. LNP, lateral neural plate; ML, midline; NP, neural plate.

the organizer requires both its DNA-binding domain and its two EH1 motifs.

We next investigated interactions between Barhl2fl, Gro4 and Tcf7l1, performing co-immunoprecipitation (Co-IP) experiments on protein extracts from transfected HEK293T cells (Fig. 3D-F). We observed that Barhl2fl co-immunoprecipitated with Gro4 (Fig. 3D). Using Tcf7l1 as bait, we observed that, in the absence of Barhl2fl, the interaction between Tcf7l1 and Gro4 could be detected with overnight Co-IP (Fig. 3E). We next tested whether Barhl2 could bind Tcf7l1, and whether it acts on formation of the Tcf7l1-Gro4 complex. We observed that Tcf7l1 co-immunoprecipitated with Barhl2fl, both in the absence and in the presence of Gro4 (Fig. 3F; lanes 2, 8). Tcf7l1 also co-immunoprecipitated with Barhl2flEHsM, which has mutated EH1 motifs (Fig. 3F; lanes 3 and 9). Thus, Barhl2 binds to Tcf7l1 independently of Gro4. Moreover, in the presence of Barhl2fl, the ability of Tcf7l1 to co-immunoprecipitate with Gro4 was increased (Fig. 3F; compare lanes 7 and 8). The effect was dependent on the EH1 motifs because Barhl2flEHsM did not promote the ability of Tcf7l1 to precipitate with Gro4 (Fig. 3F; lane 9).

We then investigated the functional consequences of the ability of Barhl2 to stabilize the Tcf7l1-Gro4 interaction. We followed the transcriptional output of the switch from repressive to active forms of Tcf induced by β-Catenin. Mean luciferase activities of pTop-Flash (Korinek et al., 1997) were measured in HEK293 T cells transfected with increasing amounts of a constitutively active form of β-Catenin (Activated-β-Cat) (Wei et al., 2003), together with a vector encoding Barhl2fl. When pTop-Flash and Activated-β-Cat were co-transfected with Barhl2fl, luciferase activity decreased at all doses of Activated-β-Cat tested, and the decrease was Barhl2-dose dependent (Fig. 3G).

Therefore, the ability of Barhl2 to limit the size of the Spemann organizer requires it to bind to DNA and an EH1-mediated protein–protein interaction. In mammalian cells, Barhl2fl interacts with Gro4 through its EH1 motifs, binds Tcf7l1 independently of Gro4, and prevents β-Catenin-driven activation of synthetic Tcf target genes.

Barhl2 limits β-Catenin-driven activation of Tcf in blastula embryos

We tested whether the ability of Barhl2 to limit β-Catenin-driven activation of Tcf target genes was conserved in blastula embryos.

We first performed Co-IP experiments using protein extracts from *Xenopus* embryos (Fig. 4A-C; Fig. S1). In *Xenopus* extracts, Gro4 co-immunoprecipitated with Barhl2fl (Fig. 4A), and Tcf7l1 co-immunoprecipitated with Barhl2 and Gro4 when injected either separately or together (Fig. 4B,C). Therefore, Barhl2 interacts with both Gro4 and Tcf7l1 in embryos.

We next investigated the effects of Barhl2 on Tcf activity during Spemann organizer development. We used a *Xenopus tropicalis* transgenic Wnt reporter line called pbin7LefdGFP (Tran et al., 2010), which contains one copy of a *wnt* reporter gene (Fig. S6). From stage 8 to stage 9.5, we observed localized Tcf activity in an area corresponding to the presumptive organizer territory (Fig. 4Da-c). Barhl2 depletion increased the number of Wnt-responsive cells in this territory (Fig. 4Ea-c). RT-qPCR quantification of the Barhl2 depletion effect demonstrated a significant increase in *gfp* mRNA levels in Barhl2-depleted embryos compared with the control at stage 8.5 (Fig. 4F). Therefore, between stage 8 and stage 9.5, Barhl2 limits the ability of Tcf to activate transcription in the presumptive organizer territory.

Development (2019) 146, dev173112. doi:10.1242/dev.173112

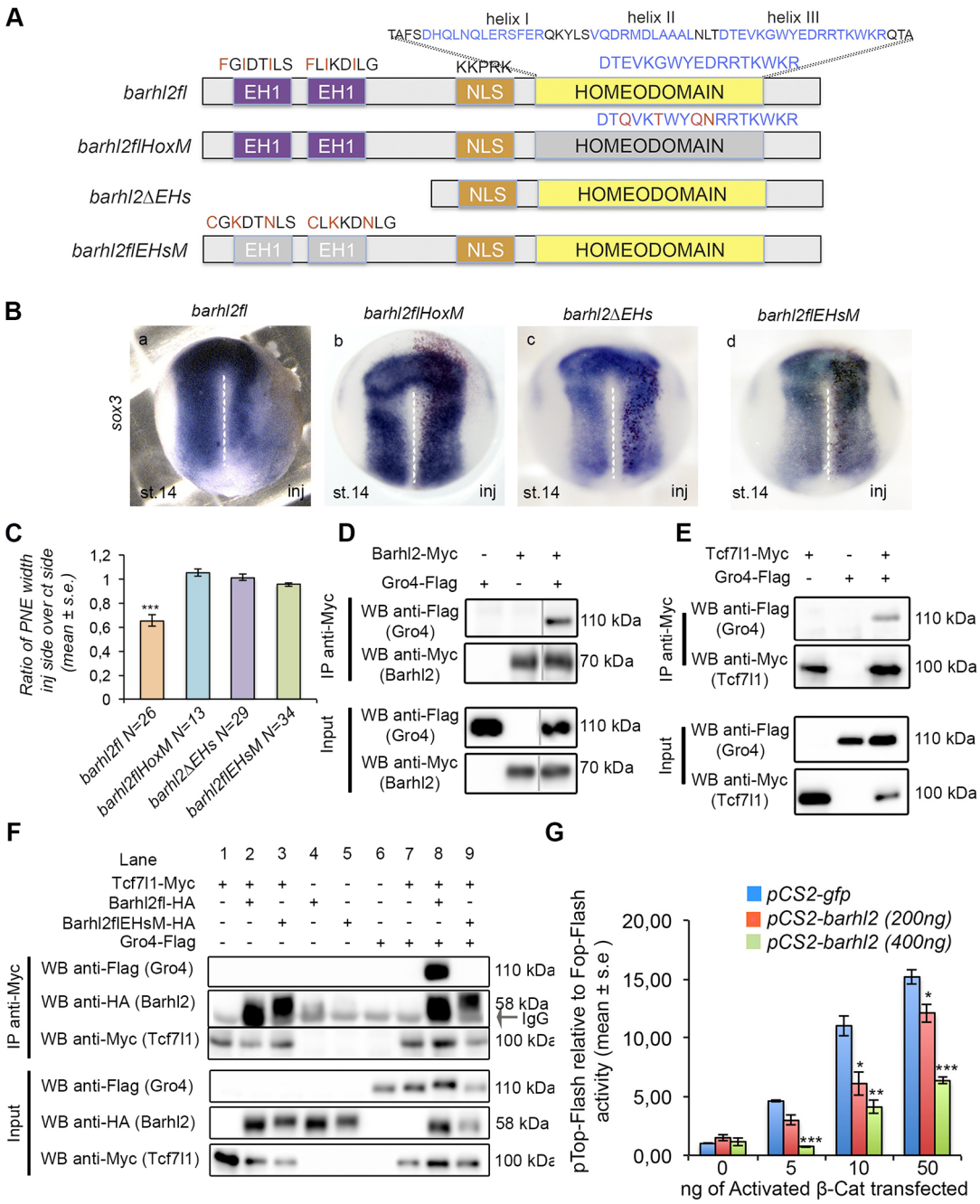

Fig. 3. Barhl2 binds to Gro and limits β-Catenin-driven Tcf transcriptional activation. (A) Scheme of *mBarhl2*-derived constructs: the AA sequences of the Homeodomain (HD) with its three helices (AAs in blue), a NLS and its two EH1 motifs. Mutated HD and EH1 motifs are shown in pale gray. (B) ISH using *sox3* as a probe in stage (st)-14 injected embryos. A dashed white line indicates the neural plate midline. (C) Quantification of B: for each embryo, the width of the posterior neuroepithelium (PNE) was measured on the injected (inj) and the control (ct) sides using ImageJ. (D-F) HEK293T cells were co-transfected with vectors (2 µg) encoding indicated proteins (Fig. S5). Co-IP was performed on cell protein extracts. Total cell lysates and the immunoprecipitated complexes were analyzed with western blot analysis. The black arrow indicates the denatured heavy chains of the anti-Myc antibody at 55 kDa. (D) Barhl2 interacts with Gro4. (E,F) Gro4 interaction with Tcf7l1 is detected either (E) when the Co-IP experiment is performed for 12 h or (F) in the presence of Barhl2fl when the Co-IP experiment is performed for 2 h. (G) HEK293T cells were transfected with increasing doses of Activated β-Catenin in the presence or absence of Barhl2. Results are shown as luciferase activity relative to Fop-Flash.

Whereas at stage 8.5, Tcf activity marked the presumptive organizer territory (Fig. 4Da-c), from stage 10 onwards, the activity of Tcf was undetectable within the dorsal blastopore lip (Fig. 4Dd, Ga). To validate our observations, we assessed the development of the dorsal blastopore lip (i.e. the organizer) upon Barhl2 LOF and GOF in stage-10.5 *X. tropicalis* transgenic Wnt reporter embryos. In agreement with a role for Barhl2 in limiting formation of the organizer, at stages 10 and 10.5, depletion of Barhl2 enlarged this area (Fig. 4Ed,Gb), whereas at stage 10.5, Barhl2 GOF dramatically decreased it (Fig. 4Gc).

Thus, we conclude that, in *Xenopus* embryos, Barhl2 interacts with both Gro4 and Tcf7l1 and, within the presumptive organizer territory, Barhl2 normally limits the activation of Tcf target genes.

Development (2019) 146, dev173112. doi:10.1242/dev.173112

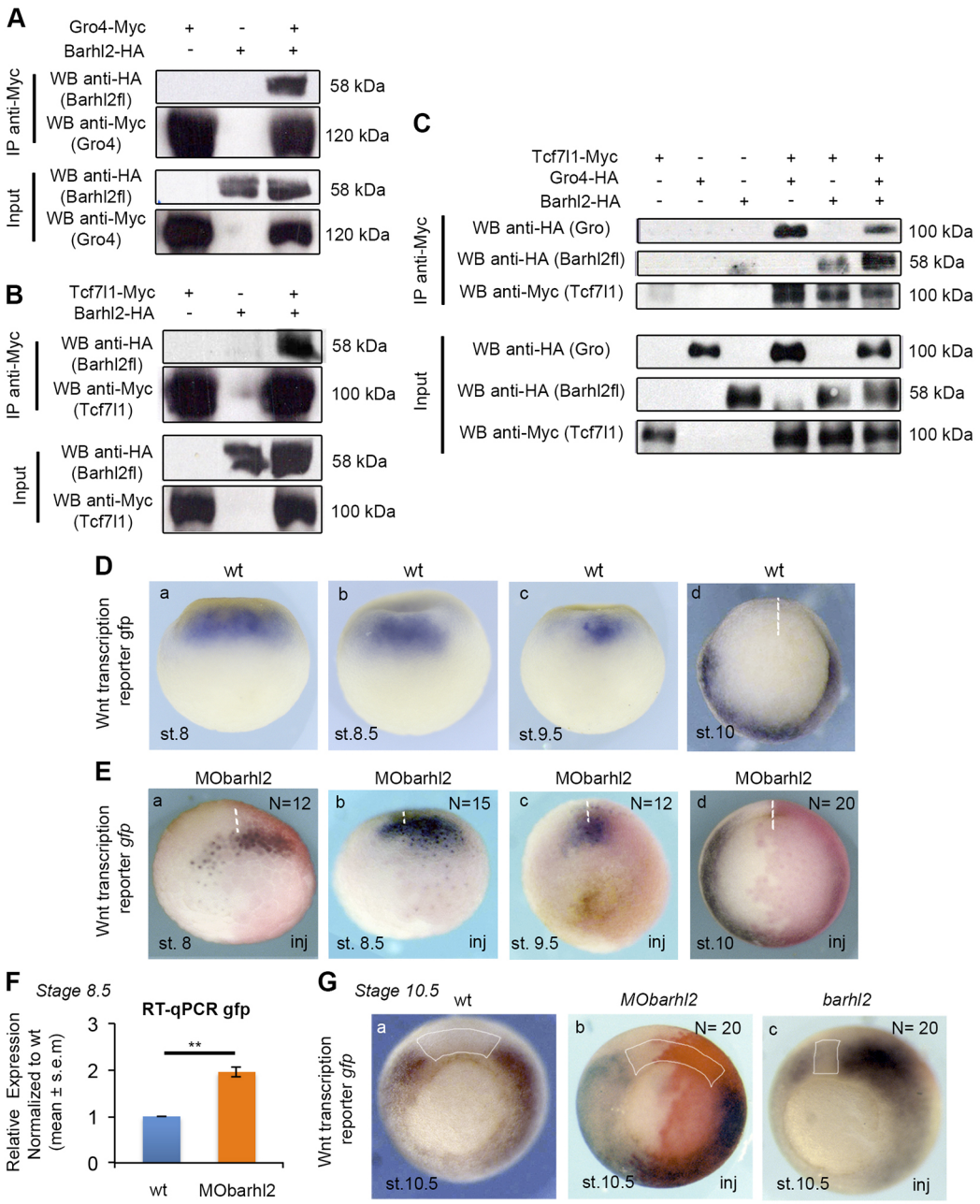

Fig. 4. Barhl2 limits β-Catenin-dependent derepression of Tcf7l1 target genes in blastula embryos. (A-C) *Xenopus* embryos were injected with RNA encoding tagged versions of Gro4, Tcf7l1 and Barhl2fl as indicated. Co-IP was performed on protein extracts from stage (st)-10 embryos. (A) Barhl2 co-immunoprecipitates with Gro. (B) Barhl2 co-immunoprecipitates with Tcf7l1. (C) Tcf7l1 co-immunoprecipitates with Gro and Barhl2 independently. (D) WT pbin7LefdGFP embryos stained for *gfp* in ISH at different developmental stages as indicated. (E) *MObarhl2* was injected in pbin7LefdGFP embryos and analyzed by ISH with *gfp* antisense probes at different stages. (F) Analysis of *gfp* levels by RT-qPCR. (G) *MObarhl2* and *mBarhl2* were injected in pbin7LefdGFP embryos, fixed at st 10.5 and analyzed by ISH with *gfp* antisense probes. A white-dotted line indicates the midline marked by tracer (red) staining. The dorsal blastopore lip is delimited by an unbroken white line. Inj, injected side.

Within the presumptive organizer territory, Barhl2 inhibits the β-Catenin-driven switch of Tcfs from inhibitor to activator

We next investigated whether Barhl2 prevents the β-Catenin-induced Tcf transcriptional switch and, consequently, the initiation of the dorsal development program.

Ventral injection of *wnt8a* RNA, which locally increases β-Catenin activity, induces duplication of the embryonic axis (McMahon and Moon, 1989; Sokol et al., 1991). Similarly, *wnt-8b*, a close paralog of *wnt8a*, can induce a secondary axis (Cui et al., 1995). We investigated the ability of Barhl2 to block this *wnt8b* induction potential (Fig. 5A,B; Fig. S7). As expected, ventral injection of *wnt8b* induced the formation of a double axis in 85% of embryos, whereas ventral injection of x*barhl2fl* or *mBarhl2fl* did not (Fig. 5A,B). However, when either x*barhl2fl* or *mBarhl2fl* was co-injected with *wnt8b*, the number of embryos developing secondary axes decreased dramatically (Fig. 5A,B). When *MObarhl2* was ventrally injected alone or with *wnt8b*, no significant impact was observed on the *wnt8b*-induced axis duplication (Fig. 5A,B). However, when co-injected with *Xbarhl2fl*, MObarhl2 completely abolished its inhibitory effect on

Development (2019) 146, dev173112. doi:10.1242/dev.173112

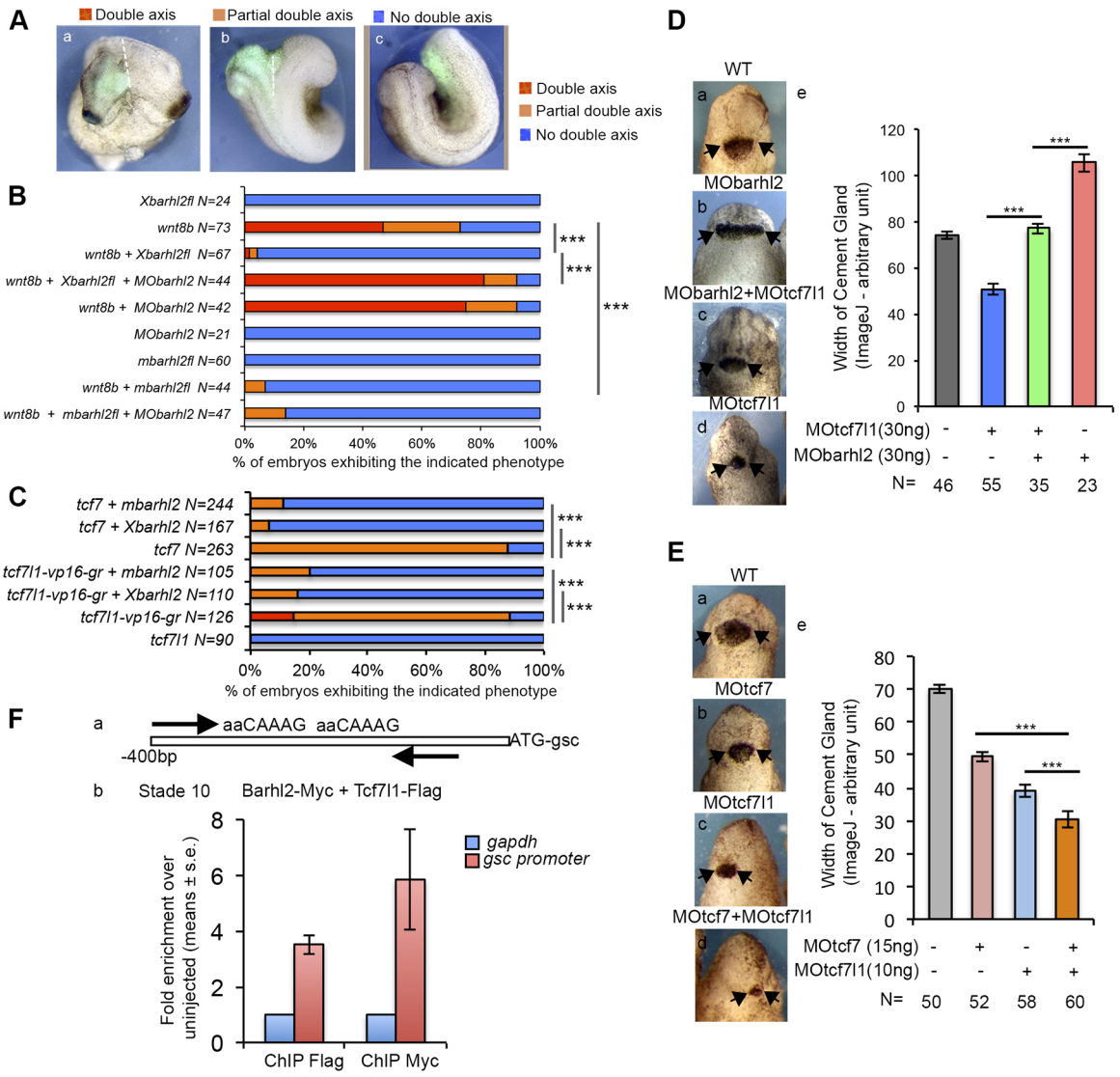

Fig. 5. Barhl2 inhibits the Tcf switch from inhibitor to activator forms while bound on DNA. (A-C) *Xenopus* embryos were injected with *wnt8b* (4 pg), *Xbarhl2* (100 pg), *mbarhl2fl* (100 pg), *tcf7* (100 pg), *tcf7l1* (100 pg), *tcf7l1vp16-GR* (100 pg) or MObarhl2 (30 ng) as indicated together with *gfp* (in green) as a tracer. (A) Representative stage-25 embryos exhibiting a (a) full (ventral view), (b) partial or (c) no double axis (dorsal view). A white-dotted line indicates the two axes. (B) Quantification of embryos exhibiting the phenotype in A when injected with *xbarhl2fl*, *wnt8b*, *mBarhl2fl* or *MObarhl2* alone or in combination in the ventral region. (C) Quantification of embryos exhibiting the phenotype in A when injected ventrally with *tcf7*, *tcf7l1*, *tcf7l1vp16-GR*, *xbarh2fl* or *mBarhl2fl* alone or in combination. (D,E) (a-d) Representative stage-25 embryos injected as indicated. (e) Quantification graph: the width of the cement gland was measured using ImageJ. The average width is indicated in arbitrary units. (F) ChIP-qPCR analysis of the promoter region of *gsc* containing Tcf-CRM (aaCAAAG). (a) Scheme of the *gsc* promoter containing two consensus Tcf-binding motifs. (b) ChIP-qPCR analysis of embryos injected with RNA encoding *barhl2-myc* and *tcf7l1-flag* using Myc or Flag antibodies as indicated. Levels of *gsc* and *gapdh* genes were quantified by qPCR. The graph represents the average fold enrichment of *gsc* relative to *gapdh* (*n*=3).

wnt8b double-axis induction. In similar conditions, and in agreement with the absence of a sequence complementary to that of *MObarhl2* in the *mBarhl2* RNA construct, *MObarhl2* had no influence on the ability of *mBarhl2* to block the inducing effect of *wnt8b* (Fig. 5A,B). Therefore, in *Xenopus* embryos, *barhl2* prevents Wnt/β-Catenin-driven activation of the Spemann organizer program.

We next investigated whether Barhl2 acts solely on Tcf7l1, or on different Tcfs, including Tcf7. In *Xenopus* embryos, between stage 7 and stage 10, transcripts encoding both *tcf7l1* and *tcf7* are detected, whereas those encoding *tcf7 like 2* (*tcf7l2*, also known as *tcf4*) and *lef1* are not (Owens et al., 2016; Session et al., 2016). Ventral injection of RNA encoding Tcf7l1 had little developmental impact (Fig. 5C). We ventrally injected RNA encoding *tcf7l1-vp16-gr*, an inducible constitutively activating form of Tcf7l1 that carries the transactivation domain of VP16 and the ligand-binding domain of the human glucocorticoid receptor (de Croze et al., 2011) (Fig. 5C). We exposed *tcf7l1-vp16-gr*-injected embryos to dexamethasone from stage 5 to stage 10 and observed formation of double axis in 89% of embryos, 16% of which had a complete double axis (Fig. 5C). Similarly, ventral injection of RNA encoding *tcf7* generated 85% of embryos with a partial double axis (Fig. 5C). Co-injection of *xbarhl2fl* or *mBarhl2fl* with either *tcf7*, or *tcf7l1-vp16-gr* significantly abolished the development of secondary axes (Fig. 5C). Therefore, Barhl2 inhibits the ability of both Tcf7 and Tcf7l1-Vp16 to induce the dorsal developmental program.

Development (2019) 146, dev173112. doi:10.1242/dev.173112

Whereas depletion of Barhl2 induced the formation of embryos with large heads and cement glands (Fig. 1; Fig. 5Da), MO-mediated inhibition of Tcf7l1 activity generated the opposite phenotype, in that Tcf7l1-depleted embryos were microcephalic (Hikasa et al., 2010) (Fig. 5Dc). To assess whether depletion of Barhl2 compensates for the depletion of Tcf7l1, we measured the cement gland width in embryos injected with either *MObarhl2* or *MOtcf7l1* or both (Fig. 5D). Depletion of both transcription factors rescued the phenotypes of both heads (Fig. 5Db,d). Using a previously validated MO for Tcf7 (Liu et al., 2005), we depleted Tcf7 either alone or together with Tcf7l1. Whereas Tcf7 depletion induced a small decrease in head and cement gland size, its co-depletion with Tcf7l1 generated an additive effect on cement gland development (Fig. 5E). Therefore, Barhl2, Tcf7 and Tcf7l1 activities participate in the induction of the dorsal program.

Finally, we investigated whether Tcf7l1 and/or Barhl2 bind to Tcf DNA-binding motifs. A 0.2-kb fragment of the *gsc* promoter contains two typical consensus Tcf *cis*-regulatory motifs (CRM), (CTTTG(A/T)(A/T)), and no Barhl2 CRM (CAATTA) (Berger et al., 2008) (Fig. 5Fa). We performed ChIP-qPCR experiments on sonicated *Xenopus* extracts injected with RNA encoding *tcf7l1-flag* together with *barhl2-myc*, using their sibling wild-type (WT) embryos as controls (Blythe et al., 2009). We performed ChIP using Myc and Flag antibodies and observed an increase in the *gsc* promoter fragment containing Tcf-CRM, compared with a fragment of the *gapdh* gene, which contains neither Tcf-CRM nor Barhl2-CRM. Therefore, both Tcf7l1 and Barhl2 can interact with the Tcf-CRM of the *gsc* promoter (Fig. 5Fb).

In conclusion, during induction of the dorsal development program, Barhl2 limits the Tcf switch from an inhibiting to an activating form, regulating both Tcf7l1 and Tcf7, probably when Tcfs are bound on DNA.

Barhl2 limits the transcription of organizer genes through Gro4-mediated repression

Taken together, our results suggested that Barhl2 switches off the early dorsal Wnt/β-Catenin response after its initial induction by *sia1*. In the blastula and early gastrula, there is an 86% correlation of CRM bound by β-Catenin and Gro co-repressors (Nakamura and Hoppler, 2017). Thus, we tested whether, at these developmental stages, Barhl2 inhibited transcription of the organizer program through Gro-mediated transcriptional repression.

To produce molecular tools that compete with Barhl2fl for Gro binding, we generated *barhl2EHs* and *barhl2EHsM* (Fig. 6A). Gro4 co-immunoprecipitated with Barhl2EHs, but not with Barhl2EHsM (Fig. S8A). Moreover, Barhl2EHs co-immunoprecipitated with Gro4 with a higher efficiency than with Gro1, arguing that Barhl2EHs interacts preferentially with Gro4 (Fig. S8B). The ability of Gro4 to co-immunoprecipitate with Barhl2EHs was also observed in embryos (Fig. S8C).

We investigated whether Barhl2EHs competes with Barhl2fl for binding to Gro4 (Fig. 5B). Using a limiting amount of Gro4 as Co-IP bait, we observed that, in the presence of Barhl2fl, increasing the amount of Barhl2EHs diminished the interaction of Gro4 with Barhl2fl (Fig. 6B, compare lane 3 to lane 5). These findings indicate that Barhl2EHs competes with Barhl2fl for Gro4 binding.

We assessed the functional consequences of Barhl2EHs interaction with Gro4 on Gro co-repressor activity. In transient transfection assays, Gro4 inhibits the activation of synthetic Tcf reporter gene transcription (Roose et al., 1998). We observed a strong decrease in pTop-Flash activity when Activated-β-Cat was co-transfected with Gro4 (Fig. 6C). This Gro-induced decrease of pTop-Flash activity was significantly alleviated in the presence of Barhl2EHs, but not in the presence of Barhl2EHsM (Fig. 6C). Using the same tools, we observed that co-transfection of Barhl2EHs reverted the inhibitory activity of Barhl2fl of Activated-β-Cat on pTop-Flash (Fig. 6D). Therefore, Barhl2EHs alleviates Gro4 and Barhl2 inhibitory activities on Tcf transcriptional activation.

We next investigated whether Barhl2 activity on organizer formation is efficiently antagonized by overexpression of its N-terminal part. At stage 14, Barhl2 depletion caused an enlargement of the neural plate (Fig. 6Ea,F). We observed that overexpression of the N-terminal part of Barhl2 (*barhl2EHs*) mimicked the Barhl2 depletion phenotype (Fig. 6Eb,F). This activity was dependent on the presence of functional EH1 motifs, because overexpression of *barhl2EHsM* did not cause any change in neural plate size (Fig. 6Ec,F). We next quantified the neural plate enlargement phenotype in embryos injected with RNAs encoding Barhl2 and/or Barhl2EHs, either separately or together. We observed that Barhl2EHs overexpression rescued the Barhl2 overexpression phenotype (Fig. 6G). Therefore, Barhl2 physiological activity is efficiently antagonized by overexpression of its N-terminal part.

Finally, we assessed Barhl2EHs activity on Spemann organizer formation. At stage 10, Barhl2EHs expanded the expression domain of the organizer markers *chd*, *gsc* and *otx2*, and shrank the expression domain of the ventrolateral mesodermal marker *vent homeobox 1* (*vent1*) in the dorsal blastopore lip area (Fig. 6H). Using *chd* and *not* as markers, we also observed that Barhl2EHs increased notochord (a derivative of the Spemann organizer) size, whereas Barhl2EHsM did not (Fig. S9). Therefore, similar to the effect of MO-mediated depletion of Barhl2 activity, Barhl2EHs overexpression increased Spemann organizer size.

Taken together, these results indicate that Barhl2 limits organizer formation through the recruitment of Gro4, which mediates transcriptional repression of the early dorsal β-Catenin signature.

Hdac1 activity participates in Barhl2-mediated transcriptional repression of organizer genes

Both Tcf and Gro interact with Hdac1 (Chen et al., 1999; Billin et al., 2000). Thus, we next tested whether Hdac1 activity participates in the Barhl2-mediated repression of organizer genes in blastula embryos.

We first investigated whether Barhl2fl influences the ability of Tcf7l1 to recruit Hdac1 and/or influences the ability of Tcf7l1 to recruit Gro4 in the presence of Hdac1. In HEK293T cells, Tcf7l1 co-immunoprecipitates with Hdac1 (Billin et al., 2000), irrespective of the presence or absence of Gro4 (Fig. 7A, lanes 4 and 5). In the presence of Hdac1, Barhl2fl increased the ability of Tcf7l1 to recruit Gro4, and Tcf7l1 co-immunoprecipitated with Barhl2fl, Gro4 and Hdac1 (Fig. 7A, lane 6). The interaction of Tcf7l1 and Barhl2fl with Hdac1 appeared to be independent of either Gro4 or the EH1 motifs, because Tcf7l1 similarly co-immunoprecipitated with Barhl2flEHsM and Hdac1 (Fig. 7A, lane 8).

These Co-IP experiments were done using an excess of Tcf7l1 as bait. Consequently, they did not indicate whether Tcf7l1 interacts with Hdac1 in a complex also containing Barhl2fl and Gro4 or, alternatively, with Hdac1 and separately with Barhl2 and Gro. In the latter case, Tcf7l1 would co-immunoprecipitate with two different protein complexes. We performed Co-IP experiments using Gro4 in limiting amounts as bait in the presence of Hdac1, Tcf7l1 and increasing amounts of Barhl2fl (Fig. 7B). When Barhl2fl was absent, Gro interacted preferentially with Hdac1 (Fig. 7B, lane 4).

Development (2019) 146, dev173112. doi:10.1242/dev.173112

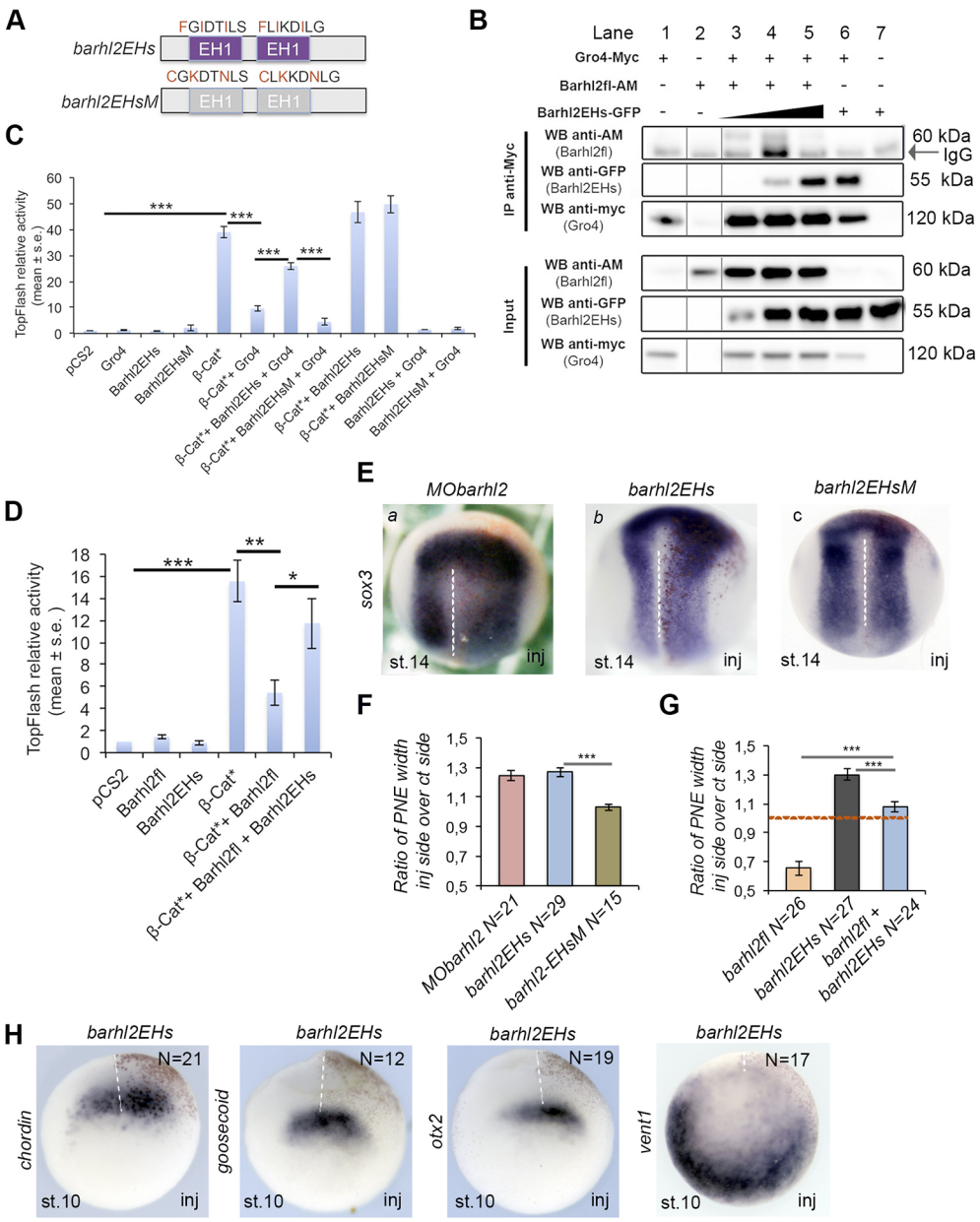

Fig. 6. The N-terminal part of Barhl2 efficiently antagonizes Barhl2fl physiological activity by buffering Gro co-repressors. (A) Scheme of *barhl2*-derived constructs. (B) HEK293T cells were co-transfected with vectors encoding indicated proteins. Gro was used as bait in a limited amount (0.5 µg) and Barhl2EHs-GFP was transfected in increasing amounts (from 0.5 to 1.5 µg). Co-IP was performed on cell protein extracts. Total cell lysates and the immunoprecipitated complexes were analyzed with western blot analysis. The black arrow indicates the denatured heavy chains of the anti-Myc antibody at 55 kDa. (C,D) HEK293T cells were transfected with plasmids encoding indicated proteins and Top-Flash activity was assessed (*n*=3). (E-G) ISH using *sox3* as a probe on stage (st)-14 embryos injected with (a) *MObarhl2*, (b) *barhl2EHs* or (c) *barhl2EHsM*. (F) Graph of quantification of E. (G) Graph quantifying the rescue experiment of the dominant-negative *barhl2EHs* on the *barh2fl* overexpression phenotype. The red-dotted line indicates a ratio of 1. (H) ISH using indicated probes on st-10 embryos injected with *barhl2EHs*. A white-dotted line indicates the midline. Inj: injected side.

In the presence of Tcf7l1 and Hdac1, interaction between Gro and Hdac1 was detected, but not between Gro and Tcf7l1 (Fig. 7B, lane 4). When the amount of Barhl2fl was increased, Gro co-immunoprecipitated with Hdac1 together with Barhl2fl and Tcf7l1 (Fig. 7B, lanes 5-7). Taken together, these observations indicate that Gro4 is part of a protein complex containing Tcf7l1, Barhl2fl and Hdac1.

We next tested whether Hdac1 activity participates in the repression of Tcf target genes in blastula embryos. We depleted Hdac1 activity using previously characterized *MOhdac1* (Tao et al., 2015), injected into pbin7LefdGFP embryos. At stage 8.5, we observed an increase in the number of Wnt-responsive cells in the Hdac1-depleted territory (Fig. 7C) as well as in the levels of *gfp* mRNA in embryos depleted for Hdac1 activity (Fig. 7D). Using RT-qPCR in individual stage-10 embryos, we observed an increase in both *chd* and *gsc* mRNA levels in embryos depleted for Hdac1 activity (Fig. 7E). Therefore, Hdac1 activity participates in transcriptional repression of organizer genes (Gao et al., 2016).

We next investigated whether Hdac1 activity contributes to Barhl2-driven transcriptional repression of organizer genes. We injected *barhl2* RNAs and *MOhdac1* either separately or together into *X. laevis* embryos and assessed organizer size by following the expression of *chd*. As previously described (Fig. 2A,B), we observed a decrease in *chd* expression in the *barhl2*-injected side of stage-10 embryos (Fig. 7Fa). By contrast, depletion of Hdac1 activity produced an enlargement of the *chd* expression territory (Fig. 7Fb). When both *MOhdac1* and *barhl2* RNA were injected together, we observed a rescue of the Barhl2 overexpression phenotype (Fig. 7Fc). We found that co-injection of *barhl2*, together with *MOhdac1*, significantly rescued the changes in organizer size (Fig. 7G; Fig. S10).

Hdac1 catalyzes the removal of acetyl groups from selected lysines in the conserved tails of core histone proteins. One of these acetylated marks is on Lysine 9 of Histone H3 (H3K9Ac) and is associated with promoters of actively transcribed genes. We tested whether Barhl2 depletion affected Hdac activity on the promoters of

Development (2019) 146, dev173112. doi:10.1242/dev.173112

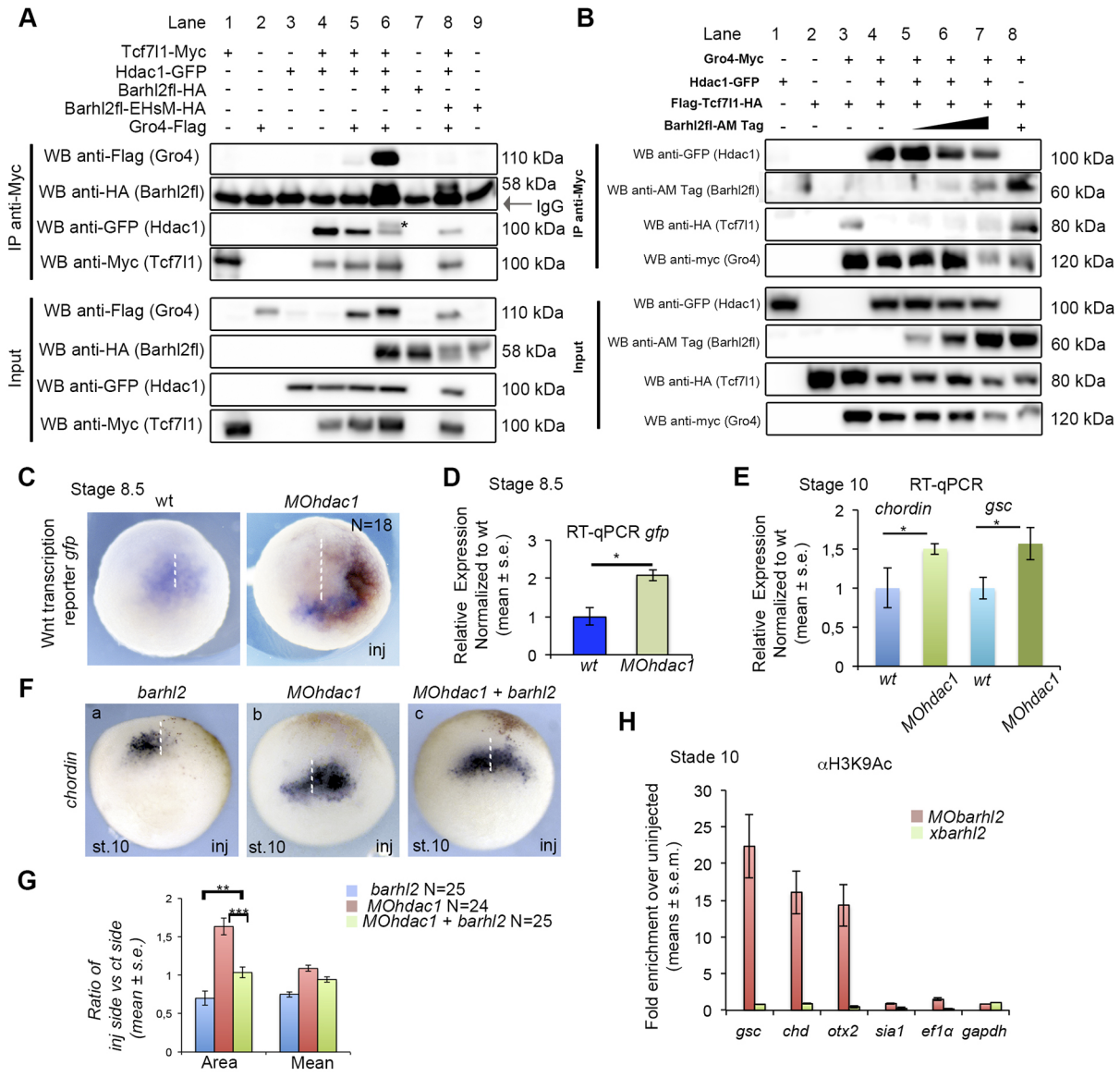

Fig. 7. Hdac1 activity participates in Barhl2 repression of the expression of key organizer genes. (A) HEK293T cells were co-transfected with vectors encoding the indicated proteins (2 µg). Co-IP was performed on cell protein extracts. Total cell lysates and the immunoprecipitated complexes were analyzed with western blot analysis. The blot membrane was first hybridized with an anti-Flag antibody (Gro4) and then with an anti-GFP antibody (Hdac1). The band marked with a black star corresponds to the leftover Gro4 signal. The black arrow indicates the denatured heavy chains of the anti-Myc antibody at 55 kDa. (B) HEK293T cells were co-transfected with vectors encoding the indicated proteins. Gro was used as a bait in a limited amount (0.5 µg) and Barhl2fl-AM was transfected in increasing amounts (from 0.5 to 1.5 µg). Co-IP was performed on cell protein extracts. Total cell lysates and the immunoprecipitated complexes were analyzed with western blot analysis. (C,D) Analysis of Hdac1 depletion in stage (st)-8.5 *Xenopus tropicalis* pbin7LefdGFP embryos using (C) ISH with *gfp* probes and (D) RT-qPCR on RNA extracts. (E) RT-qPCR analysis on *Xenopus laevis* st-10 RNA using *chordin* and *gsc* as probes on embryos depleted of Hdac1 and their WT siblings. (F) ISH using *chd* as probe in st-10 embryos injected with (a) *barhl2*, (b) *MOhdac1* and (c) *Mohdac1* and *barhl2*. (G) Quantification of the rescue experiment in F. (H) ChIP-qPCR analysis showing that depletion of Barhl2 increases H3K9Ac marks at the promoter regions of key organizer genes. Graphs represent the average relative quantification for four independent experiments. A white-dotted line indicates the midline. Inj: injected side.

the organizer genes *gsc*, *chd*, *otx2* and *sia1*. We performed ChIP-qPCR experiments on sonicated *Xenopus* extracts, either depleted of Barhl2 or injected with RNA encoding *barhl2*, using their sibling WT embryos as controls (Blythe et al., 2009). Depletion of Barhl2 induced a significant increase in the H3K9Ac marks at the promoter regions of *gsc*, *chd* and *otx2*, whereas *barhl2* overexpression did not (Fig. 7H). No changes were observed in the presence of H3K9Ac marks at the promoter of *sia1*, *ef1a* and *gapdh* (Fig. 7H). Therefore, Barhl2 depletion appears to increase the promoter activity of key organizer genes via Hdac activity.

In conclusion, at the blastula and early gastrula stages, Hdac1 activity probably participates in Barhl2-driven transcriptional repression of organizer genes.

DISCUSSION

In this study, we showed that, in both mammalian cells and *Xenopus* embryos, the transcription factor Barhl2 enhanced Tcf-mediated transcriptional repression. At the blastula and early gastrula stages, Barhl2 silenced the early, dorsal, β-Catenin transcriptional response and, consequently, limited Spemann organizer formation in time

Development (2019) 146, dev173112. doi:10.1242/dev.173112

and/or space (Fig. 8). Barhl2 repression activity was mediated via Hdac1, which is known to have a global and long-term repressive effect on transcription.

Barhl2 promotes Tcf repressive activity in cells and embryos

Whereas it had previously been proposed that β-Catenin activates Wnt-responsive genes by simply displacing Gro (Roose et al., 1998; Daniels and Weis, 2005), recent studies revealed that it promotes gene activation by displacing the whole Tcf7l1-Gro repressor complex and replacing it with an activator complex containing β-Catenin in association with Tcf7 (Roël et al., 2002; Hikasa et al., 2010) (Fig. 8). Here, we showed that Barhl2 blocked the ability of both Tcf7 and Tcf7l1 to induce axis duplication; we also provide evidence that Tcf7l1, and Tcf7 activities participated with Barhl2 in organizer formation. Thus, we propose that, during Spemann organizer formation, stabilization of β-Catenin first derepresses Tcf7l1 and then initiates the dorsal development program through activating either Tcf7 or Tcf7l1, or both. Once Barhl2 is present, it locks Tcf7l1 and/or Tcf7 in an inhibitory state (Fig. 8) and, consequently, limits induction of the dorsal development program.

In all cases, this switch from repression to activation of transcription for Wnt/β-Catenin target genes depends on the stability of the Tcf7l1-Gro repressor complex, which promotes compaction of chromatin when the canonical Wnt pathway is switched off (Shy et al., 2013). Gro co-repressors can not only attenuate gene transcription (Kaul et al., 2015), but also silence target genes by tetramerizing on a Tcf7l1-Gro complex, thereby promoting structural transitions of chromatin and transcriptional repression (Chen et al., 1998; Chodaparambil et al., 2014). In cells, Barhl2 dramatically increased Gro stoichiometry in a protein complex containing Tcf7l1 alone, or with Hdac1. Therefore, Barhl2 might promote Gro tetramerization in a complex containing Tcf7l1 and Hdac1, thereby enhancing the binding of the complex to histones and the long-term silencing of Tcf target genes.

The developmental contexts in which Tcf and/or Gro proteins mediate transcriptional silencing via Hdac activity are poorly characterized (Kaul et al., 2014; Chambers et al., 2017) (reviewed by Cinnamon and Paroush, 2008). Here, we provide evidence that Hdac1 activity contributes to Barhl2-mediated repression of canonical Wnt target genes in late blastula embryos. Our observations should help identify other developmental contexts in

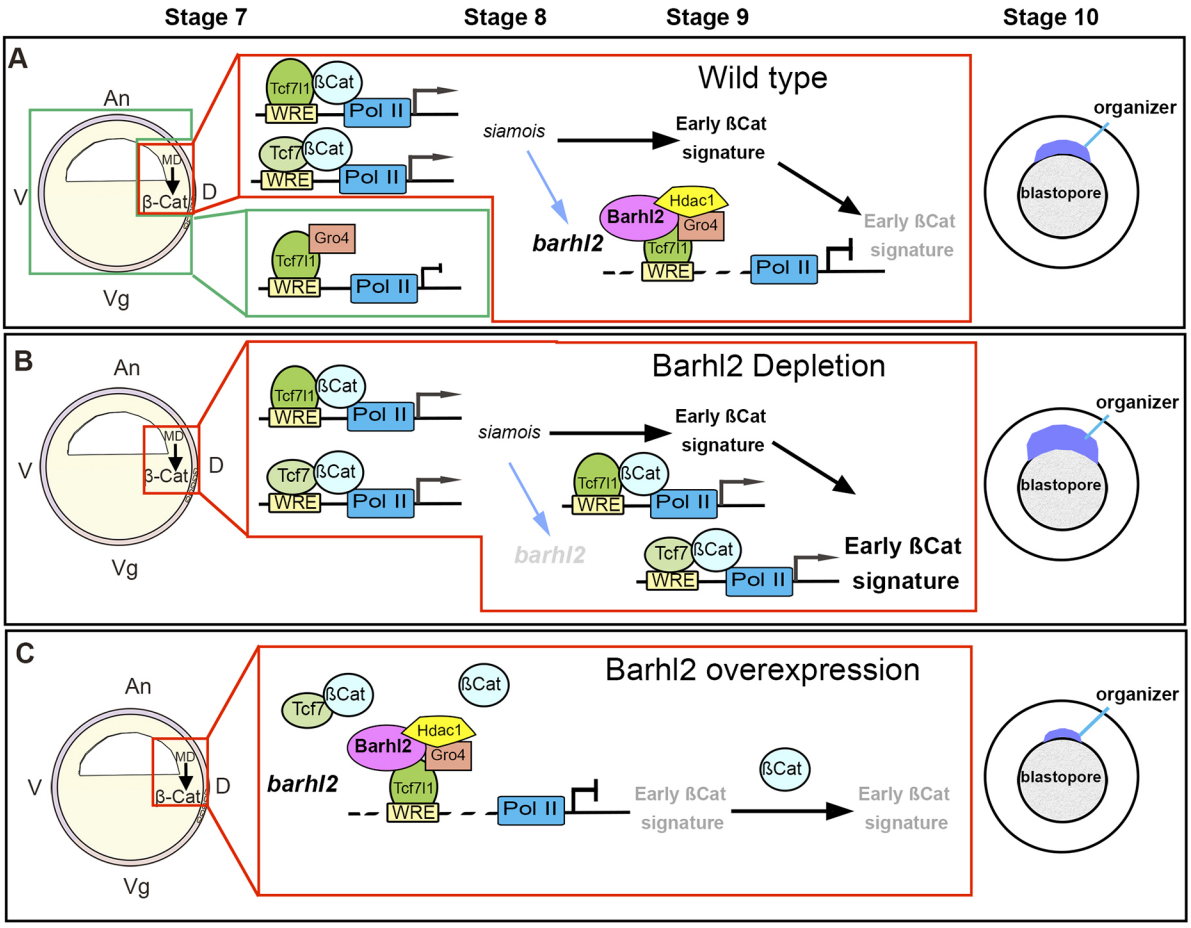

Fig. 8. Scheme of results. On the left of each part of the figure is a scheme of a stage-7 embryo. The green rectangle indicates maternally encoded Tcf7l1 with Gro repressing organizer gene transcription throughout the embryo. The red rectangle indicates that, under the influence of maternal determinants (MD), β-Catenin (β-Cat) is stabilized in the presumptive organizer territory. Tcf7l1 bound on WRE is locally derepressed. Tcf7 and/or Tcf7l1 with β-Cat bind to the WRE and induce β-Cat target genes, including *siamois*. At stage 8, β-Cat and *siamois* promote induction of the Spemann organizer. *siamois* on its own probably induces *barhl2* expression. Barhl2 holds the Gro4 and Tcf7l1 interaction, and eventually the interaction of Gro4 with Tcf7 and/or other transcription factors. A multipartite protein complex forms with Hdac1, the activity of which switches off the β-Cat response. On the right of each part of the figure is a scheme of a stage-10 embryo. The organizer is shown in blue. (A) The organizer develops within the dorsal blastopore territory. (B) Barhl2 activity is depleted, β-Cat activation is increased, and the organizer territory is enlarged. (C) Barhl2 is overexpressed, β-Cat target genes are either poorly, or not at all, transcribed and the organizer is small or does not develop. An, animal pole; D, dorsal; V, ventral; Vg, vegetal pole.

Development (2019) 146, dev173112. doi:10.1242/dev.173112

which Gro, together with Hdac1, act over long distances to silence gene transcription.

Post-transcriptional modifications, including phosphorylation and/or ubiquitination of both Tcf7l1 and Gro, can influence increase or decrease Gro-Tcf interactions (Hikasa et al., 2010; Hanson et al., 2012) (reviewed by Turki-Judeh and Courey, 2012). Although Barhl2 interacted with both Gro4 and Tcf7l1 in whole *X. laevis* embryos, it did not stabilize Gro/Tcf7l1 complexes in Co-IP experiments. It is possible that the affinity of Barhl2 for Tcfs and/or Gro is modified by post-translational modifications, which could explain the differences we observed between cells and embryos.

Barhl2 acts after the initial induction of the dorsal development program

Before stage 7.5, the dorsal accumulation of β-Catenin establishes transcriptionally poised chromatin architecture at the promoter of *sia1*, via the recruitment of the arginine methyltransferase Prmt2 (Blythe et al., 2010). Consequently, *barhl2* has no influence on the early expression of *sia1*. A study in early *X. tropicalis* gastrula revealed the presence of β-Catenin-binding sites on *sia1*, *chd*, *gsc*, *otx2*, *not* and *barhl2* loci (Nakamura et al., 2016). Whereas all the organizer genes are activated by maternal Wnt/β-Catenin signals, *barhl2* is neither part of the early dorsal β-Catenin signature nor induced by overexpression of RNA encoding *wnt8b* (Ding et al., 2017). However, injection of RNA encoding *sia1* increases *barhl2* expression (Ding et al., 2017). Given that the time window between *barhl2* and *sia1* expression is short, these findings suggest that *barhl2* is directly under the influence of *sia1*. In any case, *barhl2* starts to be expressed when the transcription of early, dorsal, β-Catenin target genes has already been initiated (Fig. 8) (Ding et al., 2017).

Barhl2 limits Spemann organizer size and signaling

In this study, we demonstrated that Barhl2 limited Spemann organizer formation. Barhl2 depletion expanded both the organizer territory and its signaling activity. It also enhanced the acetylation status of promoters of key organizer genes, thereby increasing their activity. Taken together, our results indicate that Barhl2 participates in the progression of the blastula developmental program and suggest that its physiological function is to extinguish the early dorsal Wnt/β-Catenin transcriptional wave after its initial induction by *sia1* (Fig. 8). Our results do not indicate whether *barhl2* turns off the organizer program within the entire organizer territory, or whether it acts to define the organizer boundaries.

Barhl2 switches off the early Wnt/β-Catenin response via Gro-mediated transcriptional repression

Our results argue that Barhl2EHs acts by sequestering Gro proteins and that the interaction of Barhl2 with Gro, probably Gro4, is strictly necessary for the normal activity of Barhl2. Nakamura and Hoppler demonstrated that, at these early developmental stages, Gro binds to the same CRMs as β-Catenin (Nakamura and Hoppler, 2017). A large-scale analysis identified the tissue-specific CRMs responsible for expression of head and trunk organizer genes in *Xenopus* gastrula embryos and showed that Gro represses a large battery of these genes, at least partly in association with Gsc and Otx2 (Yasuoka et al., 2014). Further studies, including RNA-seq and ChIP-seq approaches, will be necessary to establish whether Barhl2 limits the expression of organizer genes solely by enhancing Tcf repressor activity, or also by interacting with Gro in association with other transcription factors. However, our findings indicate that Barhl2 turns off the expression of most early dorsal β-Catenin target genes through its interaction with Gro.

Barhl2 activity and DNA binding

Our results suggest that, in embryos, Barhl2 acts while bound on distant enhancers and participates in gene silencing via the recruitment of Gro, together with chromatin modifiers. The gene promoters of both the pTop-Flash and the *X. tropicalis* pbin7LefdGFP Wnt reporter line do not contain Barhl2 DNA-binding motifs (Berger et al., 2008). In transfected cells, Barhl2 limited the β-Catenin activation of pTop-Flash but did not extinguish it. We suggest that, by stabilizing the Tcf7l1-Gro interaction, Barhl2 increases the pausing time of RNA polymerase II (Pol II) on the proximal promoter, a mechanism described for Gro-mediated attenuation of transcription (Kaul et al., 2015). In the *X. tropicalis* pbin7LefdGFP Wnt reporter line, Barhl2 could similarly act locally, without DNA binding. However, it could also act while bound on distant enhancers. Our ChIP-qPCR observations on the *gsc* promoter indicate that both Barhl2 and Tcf7l1 can interact with the same Tcf-CRM in the absence of an adjacent Barhl2-CRM. A form of Barhl2fl mutated for DNA binding was inactive in embryos. Further studies will be necessary to determine the contribution of the interaction of Barhl2 with DNA in the transcriptional repression process controlled by Barhl2 and Tcf. However, taken together, our observations are consistent with the long-range activity of Barhl2 via its specific binding on DNA, perhaps in superenhancers, as previously described (Lin et al., 2016).

Conclusion

Here, we described a novel mechanism by which the transcription factor Barhl2 holds the Tcf-Gro complexes in an inhibitory state. Barhl2 contributes to the Gro-mediated regulation of the chromatin state, helping to repress the transcriptional response to a given amount of Wnt signaling.

MATERIALS AND METHODS

Xenopus embryos care and husbandry

X. laevis embryos were obtained and staged using standard procedures (Nieuwkoop and Faber, 1994; Sive et al., 2010). *X. tropicalis* transgenic embryos were obtained by conventional methods of hormone-induced egg laying and *in vitro* fertilization between a WT female and a transgenic male carrying the Wnt reporter pbin7LefdGFP, as previously described (Tran et al., 2010; Tran and Vleminckx, 2014). The male was selected beforehand as having a single insertion site of the transgene (as inferred by mendelian ratios in its progeny) to insure homogeneous levels of green fluorescent protein (*gfp*) expression in the offspring (Borday et al., 2018). Experimental procedures were specifically approved by the ethics committee of the Institut Curie (Authorization 2016-013 given by CEEA-IC #118) and follow international guidelines (2010/63/UE). B.D. carries the Authorization for Vertebrates' Experimental Use N°75-1548.

Plasmids

All mutated and/or truncated forms of Barhl2 were generated from mouse *Barhl2* full-length cDNA in pCS2+ (Offner et al., 2005). The Barhl2 AA sequence is partly indicated, specifically the homeodomain (HD-60AAs) with its three helices (Fig. 3A; AAs in blue), a nuclear localization sequence (NLS) and its two EH1 domains comprising phenylalanine (F), isoleucine (I) and leucine (L). In Barhl2flHoxM, we mutated four AAs in the third helix of the homeodomain (HD-60AAs) known to interact with DNA-Q44E, T47G, Q51E and N52R. In Barhl2ΔEHs, the first 182 AAs of *Barhl2fl* were deleted. In Barhl2flEHsM, the F, I and L residues in position 1, 3 and 6 of each EH1 motif were mutated in C, K, and N, respectively. Barhl2EHs contained the first 177 AAs of mouse *Barhl2* full-length cDNA (*Barhl2fl*). In Barhl2EHsM, the AA residues in red of each EH1 motif were mutated as in Barhl2flEHsM. Constructs were generated by sequential PCR amplification followed by subcloning and sequencing in pTOPO (TOPO TA cloning kit, Thermo Fisher Scientific) and subcloned in pCS2+. The full-length and mutated cDNA tagged constructs were generated by subcloning in either pCS2-Myc (C-terminal Myc tag for Barhl2EHs-Myc and Barhl2fl-Myc), in pEGFP-N1

Development (2019) 146, dev173112. doi:10.1242/dev.173112

(N-terminal GFP tag for Barhl2fl-GFP) or in pCS2-GFP (C-terminal GFP tag for Barhl2EHs-GFP and Barhl2EHsM-GFP). HA tag (YPYDVPDYATSTIV) and AM-Tag (CQDPQRKGNVILSQAYGCQ-DPQRKGNVILSQAY)-encoding oligonucleotides were subcloned in the C termini of pCS2-*Barhl2fl* and pCS2-*Barhl2flEHsM*. HA tag-encoding oligonucleotides were subcloned in the C termini of pCS2-*groucho4* (a gift from Phil Jones, Hutchison-MRC Research Centre, Cambridge, UK). A vector carrying a Flag tag at the N-terminal end and HA (YPYDVPDYATSTIV) at the C-terminal part of Tcf7l1 was a gift from S. Sokol (Icahn School of Medicine, New York, NY, USA; Hikasa et al., 2010). pCS2+ Myc-Tcf7l1 (*Xenopus*) was a gift from Marc Kirschner (Harvard Medical School, Boston, MA, USA; Addgene plasmid #13439). p181 pK7-Hdac1 (GFP) was a gift from Ramesh Shivdasani (Dana-Farber Cancer Institute, Boston, MA, USA; Addgene plasmid #11054). pCS2+ Flag-Groucho4 and pCS2+ Myc-Groucho4 (*X. laevis*) were also gifts from Phil Jones. pCS2-XGroucho1-Flag was a gift from Nancy Papalopulu (Faculty of Life Sciences, Manchester, UK). Tc7l1p16gr was a gift from AH Monsoro Burq (de Croze et al., 2011). All necessary sequences were obtained from Xenbase (www.xenbase.org/, RRID:SCR_003280).

mRNA synthesis, antisense morpholinos and injections

Synthetic capped RNAs were prepared from pCS2+ derivatives with the mMessage mMachine kit (Ambion). Antisense oligonucleotides either with no 5′ capping or coupled to fluorescein were made by Gene Tools, as previously published: *MObarhl2 1* (15 ng) (previously *Xbarhl2ASI*), *MObarhl2 2* (30 ng) (previously *Xbarhl2ASII*), a control MO [*MObarhl2 ct* (30 ng)] had the same sequence as *MObarhl2 2*, but with five mismatches (previously *Xbarhl2ASIII*) (Offner et al., 2005), *MOhdac1* (0.3 ng) (Tao et al., 2015) and control MO *MOct* (3 ng). The effects of *MObarhl2 1* and *MObarhl2 2* were similar, but *MObarhl2 1* generated stronger developmental disruptions. We further used *MObarhl2 2* and referred to it as *MObarhl2*. The specificity of the *MObarhl2* effect has been previously demonstrated (Offner et al., 2005) with all necessary controls (reviewed in Blum et al., 2015). The MO doses we used are standard in the *Xenopus* community (Heasman et al., 2000; Liu et al., 2005; Sander et al., 2007; Hikasa et al., 2010). The overall *barhl2* mRNA sequence was conserved at 100% between *X. laevis* and *X. tropicalis* in the first 25 nucleotides on which the *MObarhl2* hybridized. We used *MObarhl2* to deplete Barhl2 activity in *X. tropicalis* embryos. We used a previously validated translation-blocking MO against the *X. laevis* Hdac1.L (Tao et al., 2015). Tao et al. performed all the necessary controls to validate the specificity and effectiveness of their MO, including the rescue experiment (Tao et al., 2015). The Hdac1 LOF phenotype we described is similar to that described by Gao et al. (2016), with two different MOs against Hdac1. Before using MOHdac1, we performed a dose-response phenotype analysis and observed toxicity effects, including gastrulation defects. We consequently chose 0.5 ng/blastomere for MOHdac1, a dose that did not induce any sign of toxicity. The hybridization site for the *X. laevis* Hdac1.L MO has only two mismatches with that of Hdac1.S and hybridizes perfectly on its last 23 nucleotides with the *X. tropicalis* Hdac1 translation initiation site sequence. Therefore, *MOHdac1* binds all *Xenopus* Hdac1 transcripts with good affinity. All sequences were obtained from Xenbase (RRID: SCR_003280). MOs were heated for 10 min at 65°C before use. Except when otherwise specified, MOs or mRNAs were co-injected with β Galactosidase (*b gal*) mRNA (100 pg) or *gfp* mRNA (100 pg) or MOct (MO standard, Gene Tools) coupled to fluorescein for lineage tracing. β Gal activity was revealed in Red-Gal (Research Organics) staining solution (Offner et al., 2005). Embryos were injected unilaterally for ISH/morphology and on both sides for RT-qPCR and ChIP-seq experiments. For all ISH analyses, three independent experiments were performed and the results were pooled. A phenotype exhibited by at least 60% of the embryos was considered significant. Except when indicated otherwise, after stage 10, the embryos are shown in dorsal view, anterior-side up. At stage 10 and below, embryos are shown in ventral view, dorsal-side up. For all rescue experiments, we tested a range of mRNA doses (50-500 pg), and selected the minimal mRNA quantity that both induced the specific phenotype and displayed no toxicity.

RT-qPCR

For each time point, an RNA extract was obtained from five individual embryos obtained from the same fertilization and the experiment was repeated at least twice. Embryos were dissociated by pipetting up and down with a 26-G needle in Trizol (Invitrogen) and extracted according to the manufacturer's instructions. RNA samples were reverse-transcribed twice, using MMLV-RT enzyme (Promega). RT-qPCR was carried out using IQ SYBR green Supermix (BioRad) on a CFX96 touch Real-Time PCR Detection System (BioRad), using standard procedures and technical triplicates for each time point. Primers were designed using Primer 3 (www.bioinformatics.nl/cgi-bin/primer3plus/primer3plus.cgi/). Primer oligomers used in qPCR are detailed in Table S1. *elongation factor 1* (*ef1*), *ornithine decarboxylase* (*odc*) and *glyceraldehyde-3-phosphate dehydrogenase* (*gapdh*) primers were used as controls when indicated.

ChIP assays

ChIP was carried out with *Xenopus* embryos at stage 10 as described by Blythe et al. (2009). Briefly, lysates of 100 injected or control embryos were crosslinked with 1% formaldehyde for 30 min at room temperature (RT). The crosslinked samples were sonicated in RIPA buffer containing 50 mM Tris-HCl pH 7.4, 1% NP-40, 0.25% Na-Deoxycholate, 150 mM NaCl, 1 mM EDTA and 0.1% SDS with a Branson sonifier 450 cell disruptor (three rounds of 20 s, intensity of 1 with a 50% duty cycle). Protein A Sepharose beads (Sigma) were used to precipitate Tcf7l1-Flag (SIGMA F3165), Barhl2-Myc (Santa Cruz 9E10), or Histone H3 acetylated K9 (Abcam 4441). After washing, protein complexes were reverse crosslinked at 65°C overnight and treated with proteinase K. DNA fragments were purified with a DNA Purification Kit (Qiagen). qPCR for the *gsc*, *chd*, *otx2*, *sia1*, *ef1* and *gapdh* promoters was performed and normalized to uninjected embryo controls according to the Applied Biosystems Protocol using SYBR Green (Thermo Fisher Scientific 659). For primers, see Table S2. Relative quantification was performed using the ΔΔC(t) method according to Blythe et al. (2009).

In situ hybridization

Control or injected embryos were collected at the indicated stages. Single ISHs were performed using digoxigenin (DIG)-labeled probes. Antisense probes were generated for *barhl2*, *sox3*, *vent2*, *chd*, *not2*, *otx2*, *gsc*, *wnt8a*, *vent1* and *gfp* according to the manufacturer's instructions (RNA Labeling Mix, Roche). *pCS2-Gfp* was a gift from David Turner (University of Michigan, Ann Arbor, MI, USA). ISH was processed following the protocol described by Juraver-Geslin et al. (2014). Briefly, following overnight incubation with the probes and then with alkaline phosphatase-conjugated anti-DIG and anti-Fluorescein (Roche) antibody, enzymatic activity was revealed using NBT/BCIP substrates (Roche). Then, bleaching treatment was performed after the postfixation of the embryos. Whole-mount images were captured using a stereomicroscope (Lumar V12). Sections (40-µm thick) were cut using a Leica VT1000 vibratome after gelatin-albumin embedding. Pictures were captured using a digital Axiocam 506 color camera on a Zeiss microscope at the PICT-IBiSA@Orsay Histology facility of Institut Curie and processed with the Zen program (version2.3), ImageJ and Adobe Photoshop CS6 software.

Firefly luciferase activity

To perform luciferase assays, HEK293T cells grown at ∼60% confluence in 24-well plates were transfected using lipofectamine (GIBCOBRL, 11668-027) with 50 ng of pTop-Flash or pFop-Flash (firefly luciferase) reporter plasmid and pCS2-β Gal as a transfection control. pTop-Flash activity was measured relative to the pFop-Flash reporter, an altered version of pTop-Flash carrying point mutations in the Tcf-binding sites to render it unresponsive to β-Catenin activity (Korinek et al., 1997). Proteins were extracted and a luciferase assay was performed according to the manufacturer's instructions (Luciferase Assay System, Promega) using a bio-luminometer TriStar LB 941 (Berthold). Firefly luciferase activity was normalized to β Gal activity (Beta-Glo Promega). The assay was performed in triplicate.

Immunoprecipitation in transfected cells and in embryos

Cells were transfected with 0.5-2 µg of expression vectors encoding tagged proteins as indicated using the Phosphate Calcium method. Plasmids coding for pCS2+ or pSK+ were used as a supplement to ensure that in the same experiment, cells in different wells were transfected with the same quantity

Development (2019) 146, dev173112. doi:10.1242/dev.173112

of expression vectors and plasmids. Thirty-six hours after transfection, cells were harvested and lysed on ice in lysis buffer containing 20 mM Tris pH7.6, 150 mM NaCl, 1% Triton, 1 mM EDTA and c0mplete™ protease inhibitor (Roche). Whole-cell lysates were cleared via centrifugation at 14,000 rpm (18,400 ***g***) for 15 min. Alternatively, 40 stage-10 embryos injected on both sides with 0.7 ng of synthetic RNA were homogenized on ice in lysis buffer containing 0.5% NP40, 5 mM EDTA, 10 mM Tris pH 7.5, 100 mM NaCl, c0mplete protease inhibitor and PhosSTOP (Sigma-Aldrich). Extracts were cleared by centrifugation for 30 min at 14,000 rpm (18,400 ***g***). In both cases, protein complexes were precipitated from the whole-cell lysates with anti-c-Myc Tag antibody (clone 9E10). Protein complexes were then precipitated with protein A-Sepharose beads (Sigma). Beads were pelleted by centrifugation and washed four times with lysis buffer. Boiling the beads in loading buffer eluted immunoprecipitates. Western blotting with cell lysates or immunoprecipitated protein elutes was performed using conventional methods. Blots were blocked with 5% milk and were detected with an ECL Western Blotting Detection Reagent (Amersham). Antibodies used are detailed in Tables S3 and S4.

Image processing

We performed the analysis on ISH of *chd*-stained *X laevis* stage-10 embryos. Separation between the control and the injected sides was based on tracer staining. To perform an objective comparison of the different expression levels of RNA by ISH, the RGB images were analyzed using an ImageJ macro (http://rsb.info.nih.gov/ij/) (Abramoff et al., 2004; Schneider et al., 2012). In such a way that the expression level is proportional to the signal recorded on the blue channel, RGB images were split and only pixel values corresponding to the blue channel were analyzed. With the goal of removing unspecific signals, background value, estimated as the average intensity of pixels outside the region of interest (ROI), were subtracted from each image. The ROI was determined by automatic segmentation using IsoData autothresholding-based determination (Ridler and Calvard, 1978). This prevents any subjectivity in ROI determination. Surface and mean pixel density on ROIs were computed for each background-corrected image. Pictures are shown corresponding to original data after histogram equalization using ImageJ with the percentage of saturated pixel 0.4. The macro is available from the authors upon request and will be available as a plug-in in ImageJ.

Statistical analysis

Except otherwise specified, all experiments were repeated at least three times. All statistical analyses were performed using the Real statistics plugin from Microsoft Excel. For both firefly luciferase activity and images analyses, the Gaussian distribution of the data between embryos for the data sets and sections of one embryo, respectively, were verified using the Shapiro Wilk statistic test. The means between two different data sets were compared using the paired sample *t*-test using the Real statistics plugin from Microsoft Excel, considering that samples were independent and variances unequal. All tests were two-tailed. *N* is the number of embryos. Significant differences are indicated in the figures with asterisks as follows: $*P \leq 0{,}05$; $**P \leq 0{,}01$; $***P \leq 0{,}001$. For all rescue experiments, the means between different data sets were compared using the Wilcoxon signed-rank test.

Acknowledgements

We thank Muriel Umbhauer, Phil Jones, Nancy Papalopulu, Muriel Perron, David Turner for gifts of materials; Sergio Marco for his advice on image processing and ImageJ macro writing; Simon Saule, Muriel Perron, Geneviève Almouzni for help and advice. The authors greatly acknowledge the PICT-IBiSA@Orsay Histology and Imaging Facilities of the Institut Curie supported by the French National Research Agency through the “Investments for the Future” program (Fran-BioImaging, ANR-10-INSB-04), the “plateau technique de biologie moléculaire” of I2BC (Véronique Henriot) for construction of plasmids, Elodie Belloir, Virginie Dangles-Marie and Isabelle Grandjean for animal care, Marion Wassef, Clemence Carron-Homo and Martin Raff for their comments on the manuscript, and Paul K. Johnson and Martin Raff for their editing work on the manuscript.

Competing interests

The authors declare no competing or financial interests.

Author contributions

Conceptualization: E.S., N.R., B.C.D.; Methodology: E.S., N.R., C.B., B.C.D.; Software: B.C.D.; Validation: E.S., N.R., C.B., B.C.D.; Formal analysis: E.S., N.R., C.B., K.P., B.C.D.; Investigation: E.S., N.R., C.B., H.S.M.A., K.P., D.S., A.C., B.C.D.; Resources: E.S., C.B., H.S.M.A., K.P., D.S., A.C., B.C.D.; Data curation: E.S., C.B., B.C.D.; Writing - original draft: B.C.D.; Writing - review & editing: E.S., N.R., C.B., K.P., B.C.D.; Visualization: B.C.D.; Supervision: B.C.D.; Project administration: B.C.D.; Funding acquisition: B.C.D.

Funding

This work was supported by the Centre National de la Recherche Scientifique (CNRS-UMR3347), the Institut National de la Santé et de la Recherche Médicale (INSERM-U1021), the Institut Curie (ETIC) and donors to B.C.D. project, the Université Paris-Sud, the Fondation Pierre-Gilles de Gennes pour la recherche (FPGG0039) and the Ligue contre le cancer (RS19/75-52). The Centre National de la Recherche Scientifique supports B.C.D. E.S. is supported by a fellowship from the Ministère de la Recherche and Association pour la Recherche sur le Cancer (DOC20170505923).

Supplementary information

Supplementary information available online at
http://dev.biologists.org/lookup/doi/10.1242/dev.173112.supplemental

References

Abramoff, M. D., Magalhaes, P. J. and Ram, S. J. (2004). Image processing with ImageJ. *Biophotonics Int.* **11**, 36-42.

Arce, L., Yokoyama, N. N. and Waterman, M. L. (2006). Diversity of LEF/TCF action in development and disease. *Oncogene* **25**, 7492-7504. doi:10.1038/sj.onc.1210056

Behrens, J., von Kries, J. P., Kühl, M., Bruhn, L., Wedlich, D., Grosschedl, R. and Birchmeier, W. (1996). Functional interaction of beta-catenin with the transcription factor LEF-1. *Nature* **382**, 638-642. doi:10.1038/382638a0

Berger, M. F., Badis, G., Gehrke, A. R., Talukder, S., Philippakis, A. A., Peña-Castillo, L., Alleyne, T. M., Mnaimneh, S., Botvinnik, O. B., Chan, E. T. et al. (2008). Variation in homeodomain DNA binding revealed by high-resolution analysis of sequence preferences. *Cell* **133**, 1266-1276. doi:10.1016/j.cell.2008.05.024

Billin, A. N., Thirlwell, H. and Ayer, D. E. (2000). Beta-catenin-histone deacetylase interactions regulate the transition of LEF1 from a transcriptional repressor to an activator. *Mol. Cell. Biol.* **20**, 6882-6890. doi:10.1128/MCB.20.18.6882-6890.2000

Blum, M., De Robertis, E. M., Wallingford, J. B. and Niehrs, C. (2015). Morpholinos: antisense and sensibility. *Dev. Cell* **35**, 145-149. doi:10.1016/j.devcel.2015.09.017

Blythe, S. A., Reid, C. D., Kessler, D. S. and Klein, P. S. (2009). Chromatin immunoprecipitation in early Xenopus laevis embryos. *Dev. Dyn.* **238**, 1422-1432. doi:10.1002/dvdy.21931

Blythe, S. A., Cha, S.-W., Tadjuidje, E., Heasman, J. and Klein, P. S. (2010). beta-Catenin primes organizer gene expression by recruiting a histone H3 arginine 8 methyltransferase, Prmt2. *Dev. Cell* **19**, 220-231. doi:10.1016/j.devcel.2010.07.007

Borday, C., Parain, K., Thi Tran, H., Vleminckx, K., Perron, M. and Monsoro-Burq, A. H. (2018). An atlas of Wnt activity during embryogenesis in Xenopus tropicalis. *PLoS ONE* **13**, e0193606. doi:10.1371/journal.pone.0193606

Brantjes, H., Roose, J., van De Wetering, M. and Clevers, H. (2001). All Tcf HMG box transcription factors interact with Groucho-related co-repressors. *Nucleic Acids Res.* **29**, 1410-1419. doi:10.1093/nar/29.7.1410

Bürglin, T. R. and Affolter, M. (2016). Homeodomain proteins: an update. *Chromosoma* **125**, 497-521. doi:10.1007/s00412-015-0543-8

Cadigan, K. M. (2012). TCFs and Wnt/beta-catenin signaling: more than one way to throw the switch. *Curr. Top. Dev. Biol.* **98**, 1-34. doi:10.1016/B978-0-12-386499-4.00001-X

Cadigan, K. M. and Waterman, M. L. (2012). TCF/LEFs and Wnt signaling in the nucleus. *Cold Spring Harb Perspect Biol.* **4**, a007906. doi:10.1101/cshperspect.a007906

Chambers, M., Turki-Judeh, W., Kim, M. W., Chen, K., Gallaher, S. D. and Courey, A. J. (2017). Mechanisms of Groucho-mediated repression revealed by genome-wide analysis of Groucho binding and activity. *BMC Genomics* **18**, 215. doi:10.1186/s12864-017-3589-6

Chen, G., Nguyen, P. H. and Courey, A. J. (1998). A role for Groucho tetramerization in transcriptional repression. *Mol. Cell. Biol.* **18**, 7259-7268. doi:10.1128/MCB.18.12.7259

Chen, G., Fernandez, J., Mische, S. and Courey, A. J. (1999). A functional interaction between the histone deacetylase Rpd3 and the corepressor groucho in Drosophila development. *Genes Dev.* **13**, 2218-2230. doi:10.1101/gad.13.17.2218

Chodaparambil, J. V., Pate, K. T., Hepler, M. R. D., Tsai, B. P., Muthurajan, U. M., Luger, K., Waterman, M. L. and Weis, W. I. (2014). Molecular functions of the TLE tetramerization domain in Wnt target gene repression. *EMBO J.* **33**, 719-731. doi:10.1002/embj.201387188

Christian, J. L. and Moon, R. T. (1993). Interactions between Xwnt-8 and Spemann organizer signaling pathways generate dorsoventral pattern in the embryonic mesoderm of Xenopus. *Genes Dev.* **7**, 13-28. doi:10.1101/gad.7.1.13
Cinnamon, E. and Paroush, Z. (2008). Context-dependent regulation of Groucho/TLE-mediated repression. *Curr. Opin. Genet. Dev.* **18**, 435-440. doi:10.1016/j.gde.2008.07.010
Clevers, H. and Nusse, R. (2012). Wnt/beta-catenin signaling and disease. *Cell* **149**, 1192-1205. doi:10.1016/j.cell.2012.05.012
Copley, R. R. (2005). The EH1 motif in metazoan transcription factors. *BMC Genomics* **6**, 169. doi:10.1186/1471-2164-6-169
Cui, Y., Brown, J. D., Moon, R. T. and Christian, J. L. (1995). Xwnt-8b: a maternally expressed Xenopus Wnt gene with a potential role in establishing the dorsoventral axis. *Development* **121**, 2177-2186.
Daniels, D. L. and Weis, W. I. (2005). Beta-catenin directly displaces Groucho/TLE repressors from Tcf/Lef in Wnt-mediated transcription activation. *Nat. Struct. Mol. Biol.* **12**, 364-371. doi:10.1038/nsmb912
de Croze, N., Maczkowiak, F. and Monsoro-Burq, A. H. (2011). Reiterative AP2a activity controls sequential steps in the neural crest gene regulatory network. *Proc. Natl. Acad. Sci. USA* **108**, 155-160. doi:10.1073/pnas.1010740107
De Robertis, E. M. and Kuroda, H. (2004). Dorsal-ventral patterning and neural induction in Xenopus embryos. *Annu. Rev. Cell Dev. Biol.* **20**, 285-308. doi:10.1146/annurev.cellbio.20.011403.154124
Ding, Y., Ploper, D., Sosa, E. A., Colozza, G., Moriyama, Y., Benitez, M. D. J., Zhang, K., Merkurjev, D. and De Robertis, E. M. (2017). Spemann organizer transcriptome induction by early beta-catenin, Wnt, Nodal, and Siamois signals in Xenopus laevis. *Proc. Natl. Acad. Sci. USA* **114**, E3081-E3090. doi:10.1073/pnas.1700766114
Eshelman, M. A., Shah, M., Raup-Konsavage, W. M., Rennoll, S. A. and Yochum, G. S. (2017). TCF7L1 recruits CtBP and HDAC1 to repress DICKKOPF4 gene expression in human colorectal cancer cells. *Biochem. Biophys. Res. Commun.* **487**, 716-722. doi:10.1016/j.bbrc.2017.04.123
Gao, L., Zhu, X., Chen, G., Ma, X., Zhang, Y., Khand, A. A., Shi, H., Gu, F., Lin, H., Chen, Y. et al. (2016). A novel role for Ascl1 in the regulation of mesendoderm formation via HDAC-dependent antagonism of VegT. *Development* **143**, 492-503. doi:10.1242/dev.126292
Hanson, A. J., Wallace, H. A., Freeman, T. J., Beauchamp, R. D., Lee, L. A. and Lee, E. (2012). XIAP monoubiquitylates Groucho/TLE to promote canonical Wnt signaling. *Mol. Cell* **45**, 619-628. doi:10.1016/j.molcel.2011.12.032
Heasman, J., Kofron, M. and Wylie, C. (2000). Beta-catenin signaling activity dissected in the early Xenopus embryo: a novel antisense approach. *Dev. Biol.* **222**, 124-134. doi:10.1006/dbio.2000.9720
Hensey, C. and Gautier, J. (1997). A developmental timer that regulates apoptosis at the onset of gastrulation. *Mech. Dev.* **69**, 183-195. doi:10.1016/S0925-4773(97)00191-3
Hensey, C. and Gautier, J. (1998). Programmed cell death during Xenopus development: a spatio-temporal analysis. *Dev. Biol.* **203**, 36-48. doi:10.1006/dbio.1998.9028
Hikasa, H., Ezan, J., Itoh, K., Li, X., Klymkowsky, M. W. and Sokol, S. Y. (2010). Regulation of TCF3 by Wnt-dependent phosphorylation during vertebrate axis specification. *Dev. Cell* **19**, 521-532. doi:10.1016/j.devcel.2010.09.005
Holland, J. D., Klaus, A., Garratt, A. N. and Birchmeier, W. (2013). Wnt signaling in stem and cancer stem cells. *Curr. Opin. Cell Biol.* **25**, 254-264. doi:10.1016/j.ceb.2013.01.004
Houston, D. W., Kofron, M., Resnik, E., Langland, R., Destree, O., Wylie, C. and Heasman, J. (2002). Repression of organizer genes in dorsal and ventral Xenopus cells mediated by maternal XTcf3. *Development* **129**, 4015-4025.
Inomata, H., Shibata, T., Haraguchi, T. and Sasai, Y. (2013). Scaling of dorsal-ventral patterning by embryo size-dependent degradation of Spemann's organizer signals. *Cell* **153**, 1296-1311. doi:10.1016/j.cell.2013.05.004
Jennings, B. H. and Ish-Horowicz, D. (2008). The Groucho/TLE/Grg family of transcriptional co-repressors. *Genome Biol.* **9**, 205. doi:10.1186/gb-2008-9-1-205
Jimenez, G., Paroush, Z. and Ish-Horowicz, D. (1997). Groucho acts as a corepressor for a subset of negative regulators, including Hairy and Engrailed. *Genes Dev.* **11**, 3072-3082. doi:10.1101/gad.11.22.3072
Juraver-Geslin, H. A., Ausseil, J. J., Wassef, M. and Durand, B. C. (2011). Barhl2 limits growth of the diencephalic primordium through Caspase3 inhibition of beta-catenin activation. *Proc. Natl. Acad. Sci. USA* **108**, 2288-2293. doi:10.1073/pnas.1014017108
Juraver-Geslin, H. A., Gómez-Skarmeta, J. L. and Durand, B. C. (2014). The conserved barH-like homeobox-2 gene barhl2 acts downstream of orthodentricle-2 and together with iroquois-3 in establishment of the caudal forebrain signaling center induced by Sonic Hedgehog. *Dev. Biol.* **396**, 107-120. doi:10.1016/j.ydbio.2014.09.027
Juraver-Geslin, H. A. and Durand, B. C. (2015). Early development of the neural plate: new roles for apoptosis and for one of its main effectors caspase-3. *Genesis* **53**, 203-224. doi:10.1002/dvg.22844
Kaul, A., Schuster, E. and Jennings, B. H. (2014). The Groucho co-repressor is primarily recruited to local target sites in active chromatin to attenuate transcription. *PLoS Genet.* **10**, e1004595. doi:10.1371/journal.pgen.1004595
Kaul, A. K., Schuster, E. F. and Jennings, B. H. (2015). Recent insights into Groucho co-repressor recruitment and function. *Transcription* **6**, 7-11. doi:10.1080/21541264.2014.1000709
Kjolby, R. A. S. and Harland, R. M. (2017). Genome-wide identification of Wnt/beta-catenin transcriptional targets during Xenopus gastrulation. *Dev. Biol.* **426**, 165-175. doi:10.1016/j.ydbio.2016.03.021
Kofron, M., Puck, H., Standley, H., Wylie, C., Old, R., Whitman, M. and Heasman, J. (2004). New roles for FoxH1 in patterning the early embryo. *Development* **131**, 5065-5078. doi:10.1242/dev.01396
Korinek, V., Barker, N., Morin, P. J., van Wichen, D., de Weger, R., Kinzler, K. W., Vogelstein, B. and Clevers, H. (1997). Constitutive transcriptional activation by a beta-catenin-Tcf complex in APC−/− colon carcinoma. *Science* **275**, 1784-1787. doi:10.1126/science.275.5307.1784
Kraus, Y., Aman, A., Technau, U. and Genikhovich, G. (2016). Pre-bilaterian origin of the blastoporal axial organizer. *Nat. Commun.* **7**, 11694. doi:10.1038/ncomms11694
Larabell, C. A., Torres, M., Rowning, B. A., Yost, C., Miller, J. R., Wu, M., Kimelman, D. and Moon, R. T. (1997). Establishment of the dorso-ventral axis in Xenopus embryos is presaged by early asymmetries in beta-catenin that are modulated by the Wnt signaling pathway. *J. Cell Biol.* **136**, 1123-1136. doi:10.1083/jcb.136.5.1123
Laugesen, A. and Helin, K. (2014). Chromatin repressive complexes in stem cells, development, and cancer. *Cell Stem Cell* **14**, 735-751. doi:10.1016/j.stem.2014.05.006
Li, H.-Y., Grifone, R., Saquet, A., Carron, C. and Shi, D.-L. (2013). The Xenopus homologue of Down syndrome critical region protein 6 drives dorsoanterior gene expression and embryonic axis formation by antagonising polycomb group proteins. *Development* **140**, 4903-4913. doi:10.1242/dev.098319
Lin, C. Y., Erkek, S., Tong, Y., Yin, L., Federation, A. J., Zapatka, M., Haldipur, P., Kawauchi, D., Risch, T., Warnatz, H.-J. et al. (2016). Active medulloblastoma enhancers reveal subgroup-specific cellular origins. *Nature* **530**, 57-62. doi:10.1038/nature16546
Liu, F., van den Broek, O., Destree, O. and Hoppler, S. (2005). Distinct roles for Xenopus Tcf/Lef genes in mediating specific responses to Wnt/beta-catenin signalling in mesoderm development. *Development* **132**, 5375-5385. doi:10.1242/dev.02152
McMahon, A. P. and Moon, R. T. (1989). Ectopic expression of the proto-oncogene int-1 in Xenopus embryos leads to duplication of the embryonic axis. *Cell* **58**, 1075-1084. doi:10.1016/0092-8674(89)90506-0
Milet, C., Maczkowiak, F., Roche, D. D. and Monsoro-Burq, A. H. (2013). Pax3 and Zic1 drive induction and differentiation of multipotent, migratory, and functional neural crest in Xenopus embryos. *Proc. Natl. Acad. Sci. USA* **110**, 5528-5533. doi:10.1073/pnas.1219124110
Molenaar, M., van de Wetering, M., Oosterwegel, M., Peterson-Maduro, J., Godsave, S., Korinek, V., Roose, J., Destrée, O. and Clevers, H. (1996). XTcf-3 transcription factor mediates beta-catenin-induced axis formation in Xenopus embryos. *Cell* **86**, 391-399. doi:10.1016/S0092-8674(00)80112-9
Nakamura, Y. and Hoppler, S. (2017). Genome-wide analysis of canonical Wnt target gene regulation in Xenopus tropicalis challenges beta-catenin paradigm. *Genesis* **55**, e22991. doi:10.1002/dvg.22991
Nakamura, Y., de Paiva Alves, E., Veenstra, G. J. C. and Hoppler, S. (2016). Tissue- and stage-specific Wnt target gene expression is controlled subsequent to beta-catenin recruitment to cis-regulatory modules. *Development* **143**, 1914-1925. doi:10.1242/dev.131664
Niehrs, C. (2004). Regionally specific induction by the Spemann-Mangold organizer. *Nat. Rev. Genet.* **5**, 425-434. doi:10.1038/nrg1347
Nieuwkoop, P. D. and Faber, J., eds (1994). *Normal Table of Xenopus Laevis (Daudin): a Systematical and Chronological Survey of the Development from the Fertilized Egg Till the End of Metamorphosis*. New York: Garland.
Nusse, R. and Clevers, H. (2017). Wnt/beta-catenin signaling, disease, and emerging therapeutic modalities. *Cell* **169**, 985-999. doi:10.1016/j.cell.2017.05.016
Offner, N., Duval, N., Jamrich, M. and Durand, B. (2005). The pro-apoptotic activity of a vertebrate Bar-like homeobox gene plays a key role in patterning the Xenopus neural plate by limiting the number of chordin- and shh-expressing cells. *Development* **132**, 1807-1818. doi:10.1242/dev.01712
Owens, N. D. L., Blitz, I. L., Lane, M. A., Patrushev, I., Overton, J. D., Gilchrist, M. J., Cho, K. W. and Khokha, M. K. (2016). Measuring absolute RNA copy numbers at high temporal resolution reveals transcriptome kinetics in development. *Cell Rep.* **14**, 632-647. doi:10.1016/j.celrep.2015.12.050
Pickles, L. M., Roe, S. M., Hemingway, E. J., Stifani, S. and Pearl, L. H. (2002). Crystal structure of the C-terminal WD40 repeat domain of the human Groucho/TLE1 transcriptional corepressor. *Structure* **10**, 751-761. doi:10.1016/S0969-2126(02)00768-2
Ramakrishnan, A. B., Sinha, A., Fan, V. B. and Cadigan, K. M. (2018). The Wnt transcriptional switch: TLE removal or inactivation? *BioEssays* **40**, 1700162. doi:10.1002/bies.201700162
Ridler, T. W. and Calvard, S. (1978). Picture thresholding using an iterative selection method. *IEEE Trans. Syst. Man Cybern.* **8**, 630-632. doi:10.1109/TSMC.1978.4310039

Roël, G., Hamilton, F. S., Gent, Y., Bain, A. A., Destrée, O. and Hoppler, S. (2002). Lef-1 and Tcf-3 transcription factors mediate tissue-specific Wnt signaling during Xenopus development. *Curr. Biol.* **12**, 1941-1945. doi:10.1016/S0960-9822(02)01280-0

Roose, J., Molenaar, M., Peterson, J., Hurenkamp, J., Brantjes, H., Moerer, P., van de Wetering, M., Destrée, O. and Clevers, H. (1998). The Xenopus Wnt effector XTcf-3 interacts with Groucho-related transcriptional repressors. *Nature* **395**, 608-612. doi:10.1038/26989

Sander, V., Reversade, B. and De Robertis, E. M. (2007). The opposing homeobox genes Goosecoid and Vent1/2 self-regulate Xenopus patterning. *EMBO J.* **26**, 2955-2965. doi:10.1038/sj.emboj.7601705

Schneider, S., Steinbeisser, H., Warga, R. M. and Hausen, P. (1996). Beta-catenin translocation into nuclei demarcates the dorsalizing centers in frog and fish embryos. *Mech. Dev.* **57**, 191-198. doi:10.1016/0925-4773(96)00546-1

Schneider, C. A., Rasband, W. S. and Eliceiri, K. W. (2012). NIH Image to ImageJ: 25 years of image analysis. *Nat. Methods* **9**, 671-675. doi:10.1038/nmeth.2089

Schuhmacher, L.-N., Albadri, S., Ramialison, M. and Poggi, L. (2011). Evolutionary relationships and diversification of barhl genes within retinal cell lineages. *BMC Evol. Biol.* **11**, 340. doi:10.1186/1471-2148-11-340

Schuijers, J., Mokry, M., Hatzis, P., Cuppen, E. and Clevers, H. (2014). Wnt-induced transcriptional activation is exclusively mediated by TCF/LEF. *EMBO J.* **33**, 146-156. doi:10.1002/embj.201385358

Sena, E., Feistel, K. and Durand, B. C. (2016). 'An evolutionarily conserved network mediates development of the zona limitans intrathalamica, a sonic hedgehog-secreting caudal forebrain signaling center. *J. Dev. Biol.* **4**, 31. doi:10.3390/jdb4040031

Session, A. M., Uno, Y., Kwon, T., Chapman, J. A., Toyoda, A., Takahashi, S., Fukui, A., Hikosaka, A., Suzuki, A., Kondo, M. et al. (2016). Genome evolution in the allotetraploid frog Xenopus laevis. *Nature* **538**, 336-343. doi:10.1038/nature19840

Seto, E. and Yoshida, M. (2014). Erasers of histone acetylation: the histone deacetylase enzymes. *Cold Spring Harb Perspect Biol.* **6**, a018713. doi:10.1101/cshperspect.a018713

Shy, B. R., Wu, C.-I., Khramtsova, G. F., Zhang, J. Y., Olopade, O. I., Goss, K. H. and Merrill, B. J. (2013). Regulation of Tcf7l1 DNA binding and protein stability as principal mechanisms of Wnt/beta-catenin signaling. *Cell Rep.* **4**, 1-9. doi:10.1016/j.celrep.2013.06.001

Sive, H. L., Grainger, R. M. and Harland, R. M. (2010). Microinjection of Xenopus embryos. *Cold Spring Harb. Protoc.* **2010**, pdb ip81. doi:10.1101/pdb.ip81

Smith, S. T. and Jaynes, J. B. (1996). A conserved region of engrailed, shared among all en-, gsc-, Nk1-, Nk2- and msh-class homeoproteins, mediates active transcriptional repression in vivo. *Development* **122**, 3141-3150.

Sokol, S. Y. (2011). Maintaining embryonic stem cell pluripotency with Wnt signaling. *Development* **138**, 4341-4350. doi:10.1242/dev.066209

Sokol, S., Christian, J. L., Moon, R. T. and Melton, D. A. (1991). Injected Wnt RNA induces a complete body axis in Xenopus embryos. *Cell* **67**, 741-752. doi:10.1016/0092-8674(91)90069-B

Stern, C. D. (2006). Neural induction: 10 years on since the 'default model'. *Curr. Opin. Cell Biol.* **18**, 692-697. doi:10.1016/j.ceb.2006.09.002

Tao, Q., Yokota, C., Puck, H., Kofron, M., Birsoy, B., Yan, D., Asashima, M., Wylie, C. C., Lin, X. and Heasman, J. (2005). Maternal wnt11 activates the canonical wnt signaling pathway required for axis formation in Xenopus embryos. *Cell* **120**, 857-871. doi:10.1016/j.cell.2005.01.013

Tao, Y., Ruan, H., Guo, X., Li, L. and Shen, W. (2015). HDAC1 regulates the proliferation of radial glial cells in the developing Xenopus tectum. *PLoS ONE* **10**, e0120118. doi:10.1371/journal.pone.0120118

Tran, H. T. and Vleminckx, K. (2014). Design and use of transgenic reporter strains for detecting activity of signaling pathways in Xenopus. *Methods* **66**, 422-432. doi:10.1016/j.ymeth.2013.06.028

Tran, H. T., Sekkali, B., Van Imschoot, G., Janssens, S. and Vleminckx, K. (2010). Wnt/beta-catenin signaling is involved in the induction and maintenance of primitive hematopoiesis in the vertebrate embryo. *Proc. Natl. Acad. Sci. USA* **107**, 16160-16165. doi:10.1073/pnas.1007725107

Turki-Judeh, W. and Courey, A. J. (2012). Groucho: a corepressor with instructive roles in development. *Curr. Top. Dev. Biol.* **98**, 65-96. doi:10.1016/B978-0-12-386499-4.00003-3

Wei, Y., Renard, C.-A., Labalette, C., Wu, Y., Lévy, L., Neuveut, C., Prieur, X., Flajolet, M., Prigent, S. and Buendia, M.-A. (2003). Identification of the LIM protein FHL2 as a coactivator of beta-catenin. *J. Biol. Chem.* **278**, 5188-5194. doi:10.1074/jbc.M207216200

Xanthos, J. B., Kofron, M., Tao, Q., Schaible, K., Wylie, C. and Heasman, J. (2002). The roles of three signaling pathways in the formation and function of the Spemann Organizer. *Development* **129**, 4027-4043.

Yasuoka, Y., Suzuki, Y., Takahashi, S., Someya, H., Sudou, N., Haramoto, Y., Cho, K. W., Asashima, M., Sugano, S. and Taira, M. (2014). Occupancy of tissue-specific cis-regulatory modules by Otx2 and TLE/Groucho for embryonic head specification. *Nat. Commun.* **5**, 4322. doi:10.1038/ncomms5322

Yeo, W. and Gautier, J. (2003). A role for programmed cell death during early neurogenesis in xenopus. *Dev. Biol.* **260**, 31-45. doi:10.1016/S0012-1606(03)00222-7

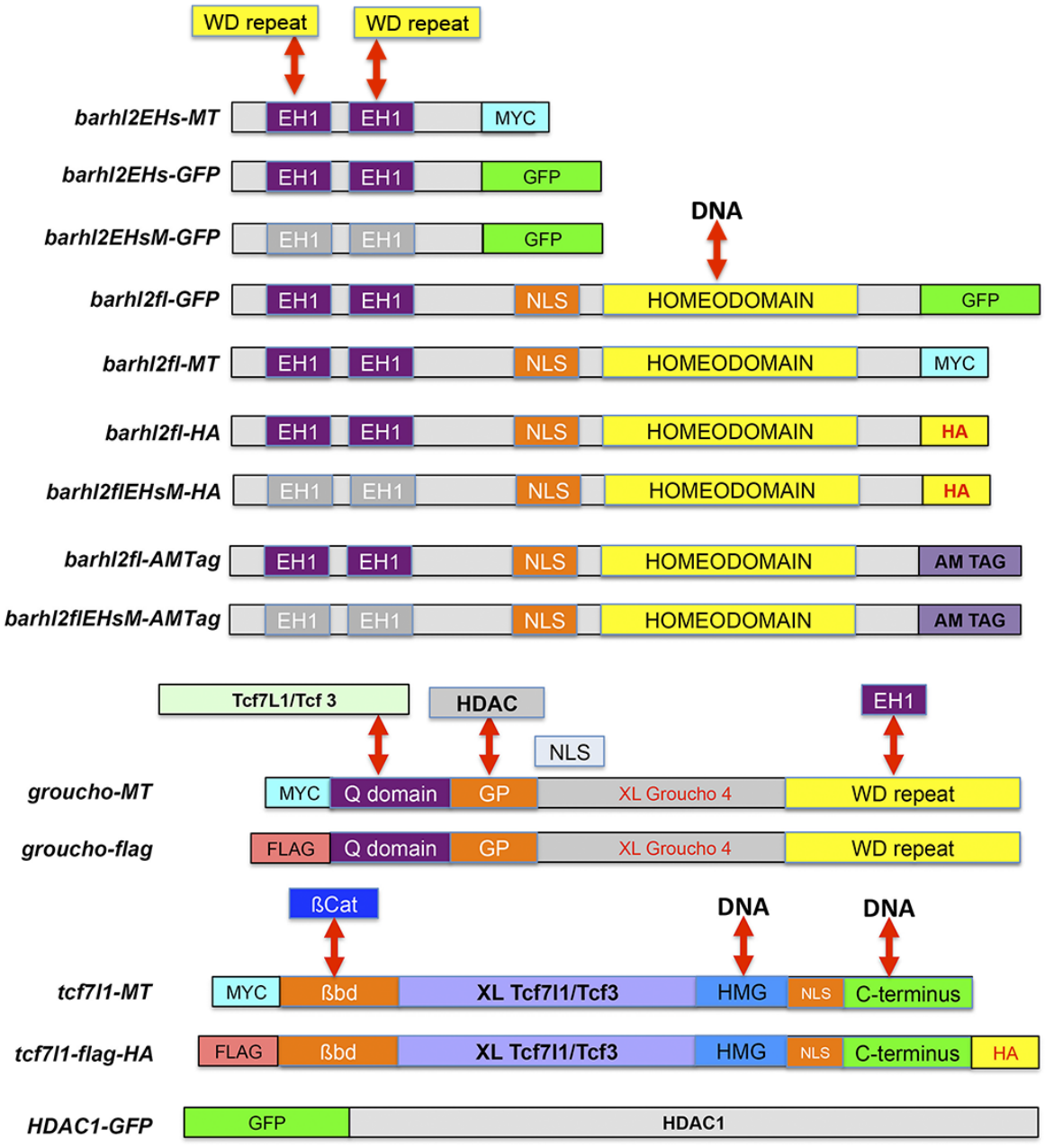

Figure S1: Scheme of tagged constructs used. Scheme of 1: Barhl2 cDNA derived constructs carrying Myc, GFP, HA and AM tags in their C-terminal end as indicated; 2: *X. laevis* Gro4 carrying Myc, HA or Flag tag at their N-terminal or C-terminal end as indicated; 3: *X. laevis* Tcf7l1 carrying Myc, HA or Flag tag at their N-terminal or C-terminal end as indicated; 4- human Hdac1 carrying GFP tag at its N-terminal end. The double arrows indicate domains of protein-protein or protein-DNA interactions.

Figure S2: Quantification of Figure 2A *chordin* staining. The top panel corresponds to the injected side. All analyzed embryos are shown. The control and injected sides were delimited based on tracer. The top panel corresponds to the injected side. For each RGB image every step of the imageJ analysis protocol is shown. From left to right: RGB images centered on the region of interest (ROI) control and injected sides; blue channel of the RGB image; Blue channel minus the background value, estimated as the average intensity of pixels outside the ROI; Area considered for pixels quantification. Pictures correspond to original data after histogram equalization using ImageJ with percentage of saturated pixel 0.4. (A) embryos injected with *barhl2fl*. (B) embryos injected with *MObarhl2-ct*. (C) embryos injected with *MObarhl2*.

Figure S2A: Embryos injected with *Xbarhl2fl*.

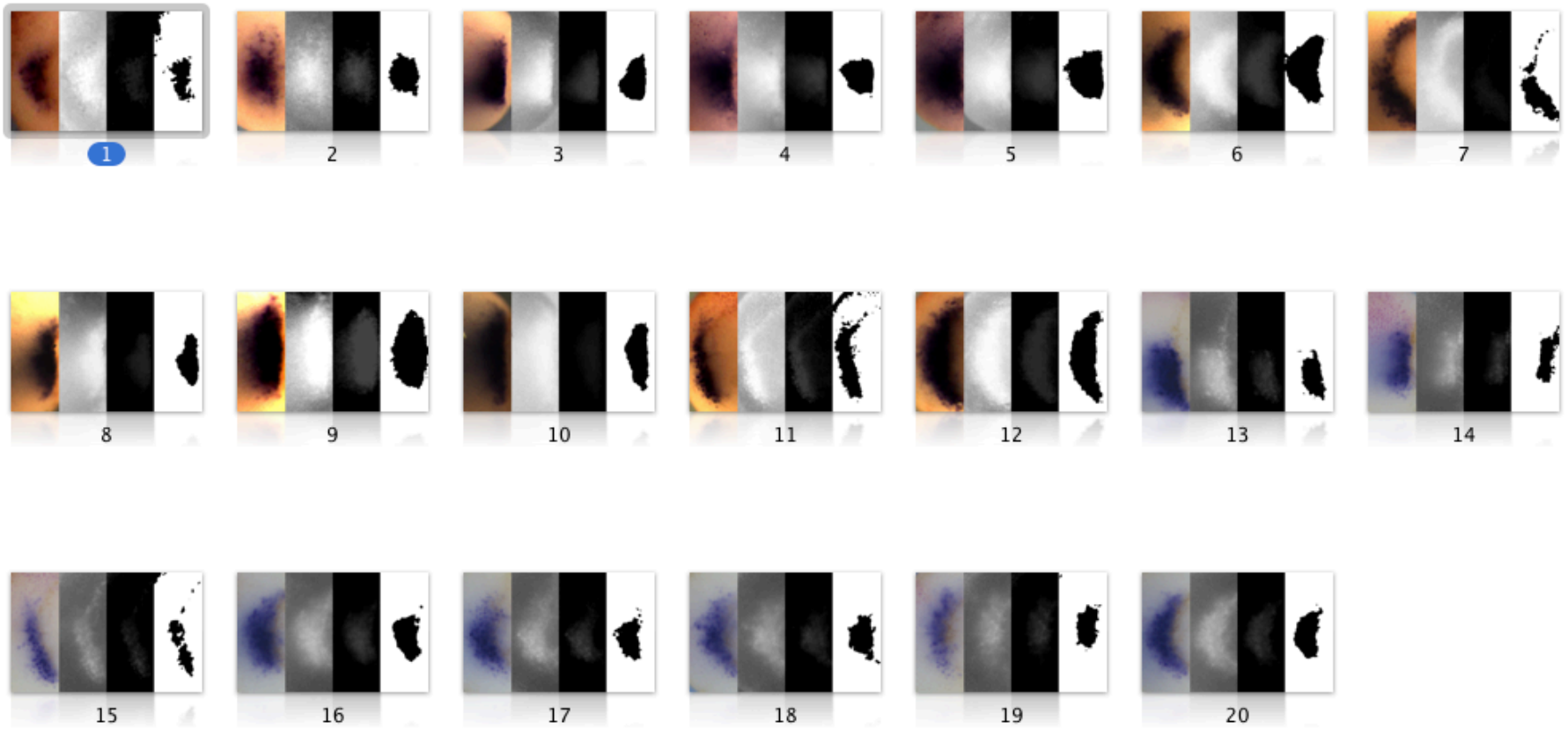

Figure S2B: Embryos injected with *MObarhl2-ct*.

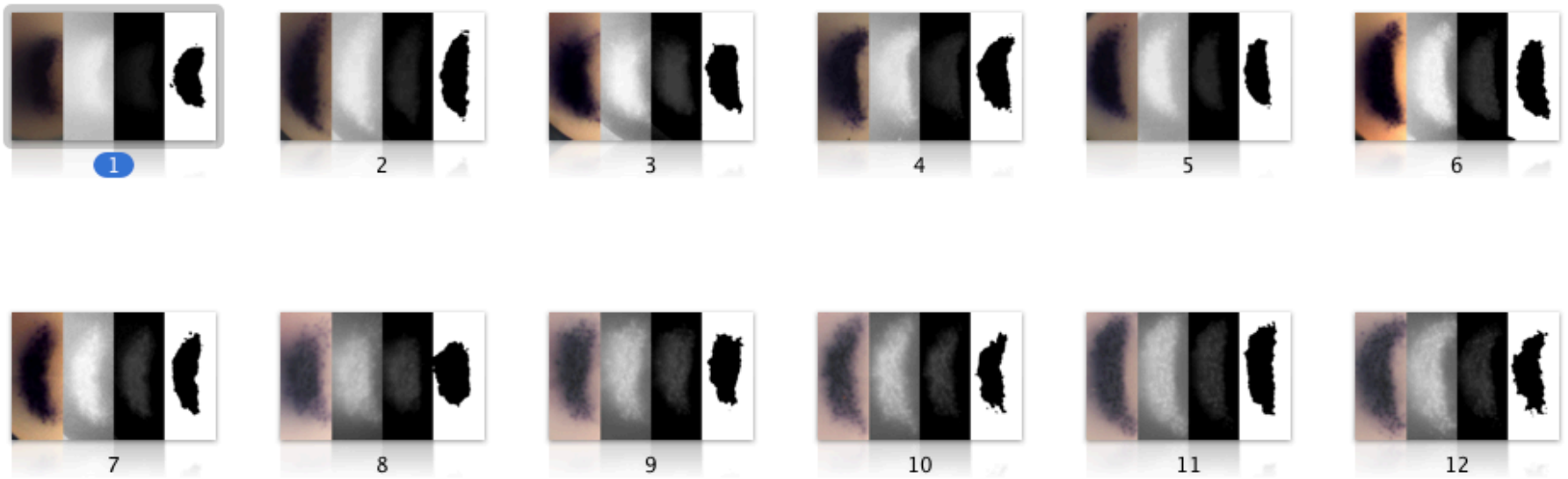

Figure S2C: Embryos injected with *MObarhl2*.

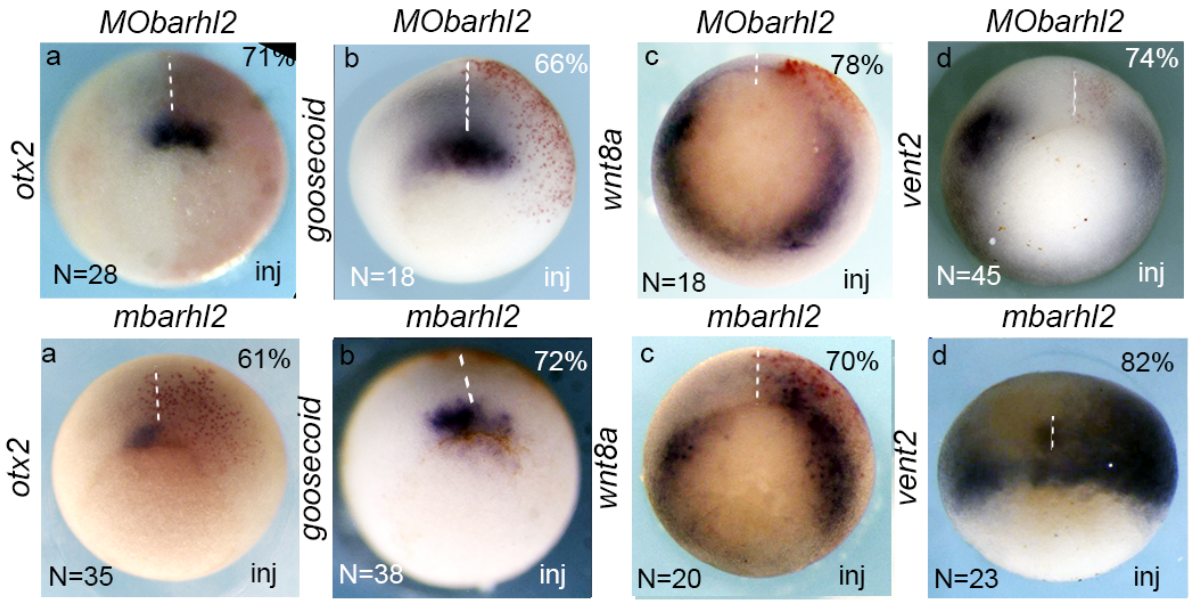

Figure S3: (A) ISH on embryos depleted for Barhl2 (*MObarhl2*) at stage (st) 10.5 using (a) *otx2*, (b) *goosecoid*, (c) *wnt8a* or (d) *vent2* as probes. (B) ISH on embryos injected with *barhl2* at stage (st) 10.5 using (a) *otx2*, (b) *goosecoid*, (c) *wnt8a* or (d) *vent2* as probes. Representative *X. laevis* embryos are shown ventral view dorsal up. Embryos were injected together with a tracer (in red) to assess area of injection. The number of embryos injected (N), as the percentage of embryos exhibiting the phenotype are indicated. inj: injected side. a white dotted line indicates the midline.

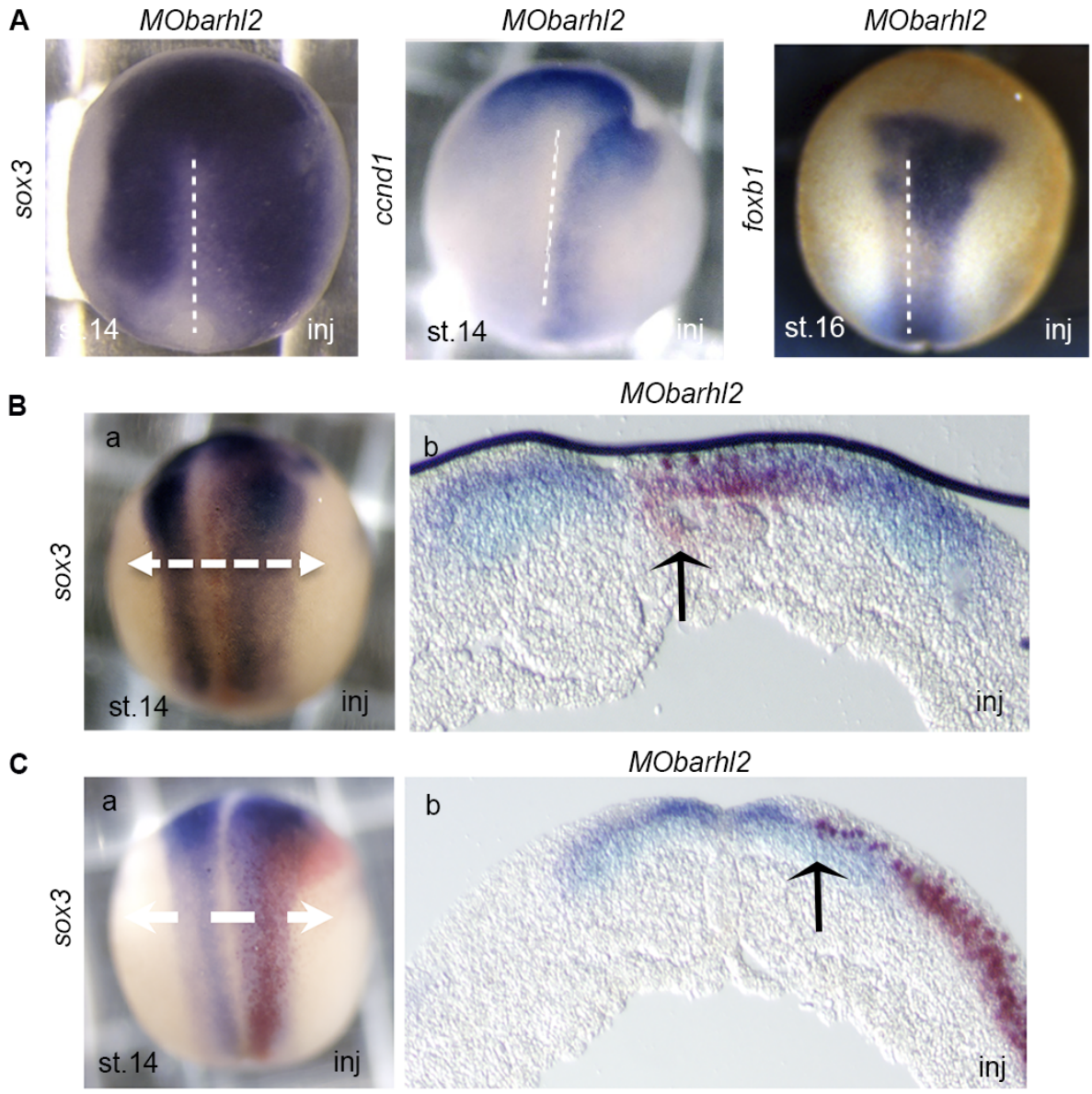

Figure S4: (A) ISH on embryos depleted for Barhl2 (*MObarhl2*) using *sox3*, an early marker of the neural plate, *foxb1*, a marker of hindbrain and diencephalic territories (Gamse and Sive, 2001) and *ccnd1*, which is regulated by both Shh and Wnt signaling (Borday et al., 2012), as probes. Representative embryos are shown dorsal view, anterior up. (B, C) ISH on embryos depleted for Barhl2 (*MObarhl2*) using *sox3* as a probe. Representative embryos in which Barhl2 activity was depleted either (Ba) in the dorsal mesoderm (future organizer) and axial dorsal ectoderm (floor plate), (Ca) or in lateral mesoderm and lateral ectoderm are shown in dorsal view, anterior up, together with representative transverse sections (50µm) at the AP axis positions indicated with a white-dashed arrow (Bb; Cb). Embryos were injected together with a tracer (in red) to assess are of injection. The black arrow indicates the limits of the injected territory. inj: injected side. st: stage.

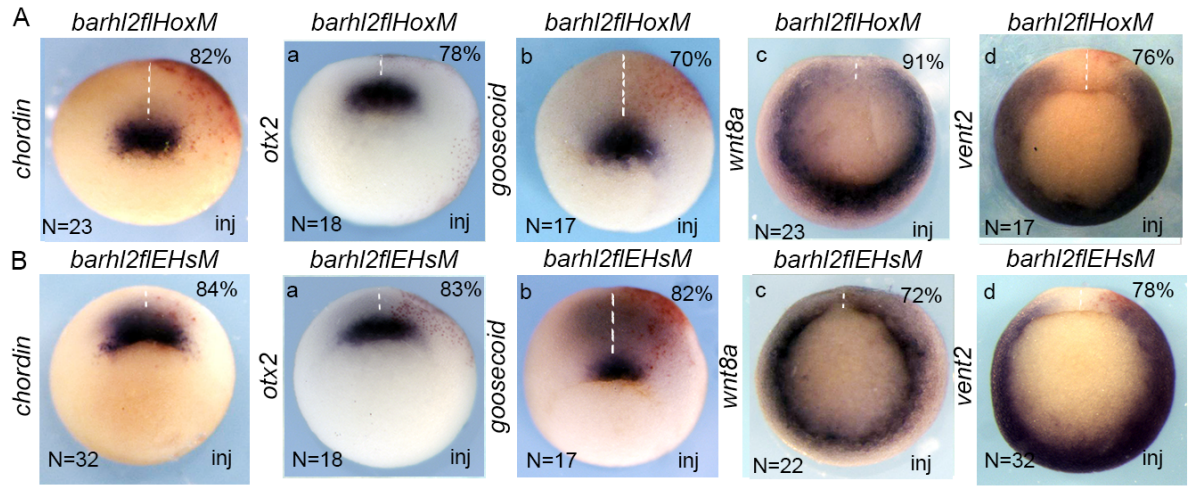

Figure S5: (A, B) ISH on embryos injected with *BarhI2flHoxM (A), or BarhI2flEHsM* (B) at stage (st) 10.5 using (a) *chordin*, (b) *otx2*, (c) *goosecoid*, (d) *wnt8a* or (e) *vent2* as probes. Representative *X. laevis* embryos are shown ventral view dorsal up. Embryos were injected together with a tracer (in red) to assess area of injection. The number of embryos injected (N), as the percentage of embryos exhibiting the phenotype are indicated. inj: injected side. a white dotted line indicates the midline.

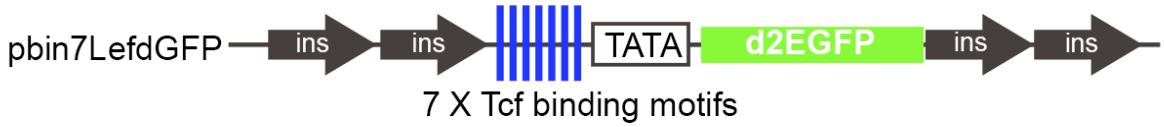

Figure S6: Scheme of the transgene Wnt reporter construct; The construct contains chicken β-globin insulators and seven Tcf consensus binding sites driving expression of a destabilized eGFP. This line allows a read-out of Wnt/Tcf activity in vivo, through either ISH using a gfp antisense probe or RT-qPCR for gfp (Tran et al., 2010; Borday et al., 2018).

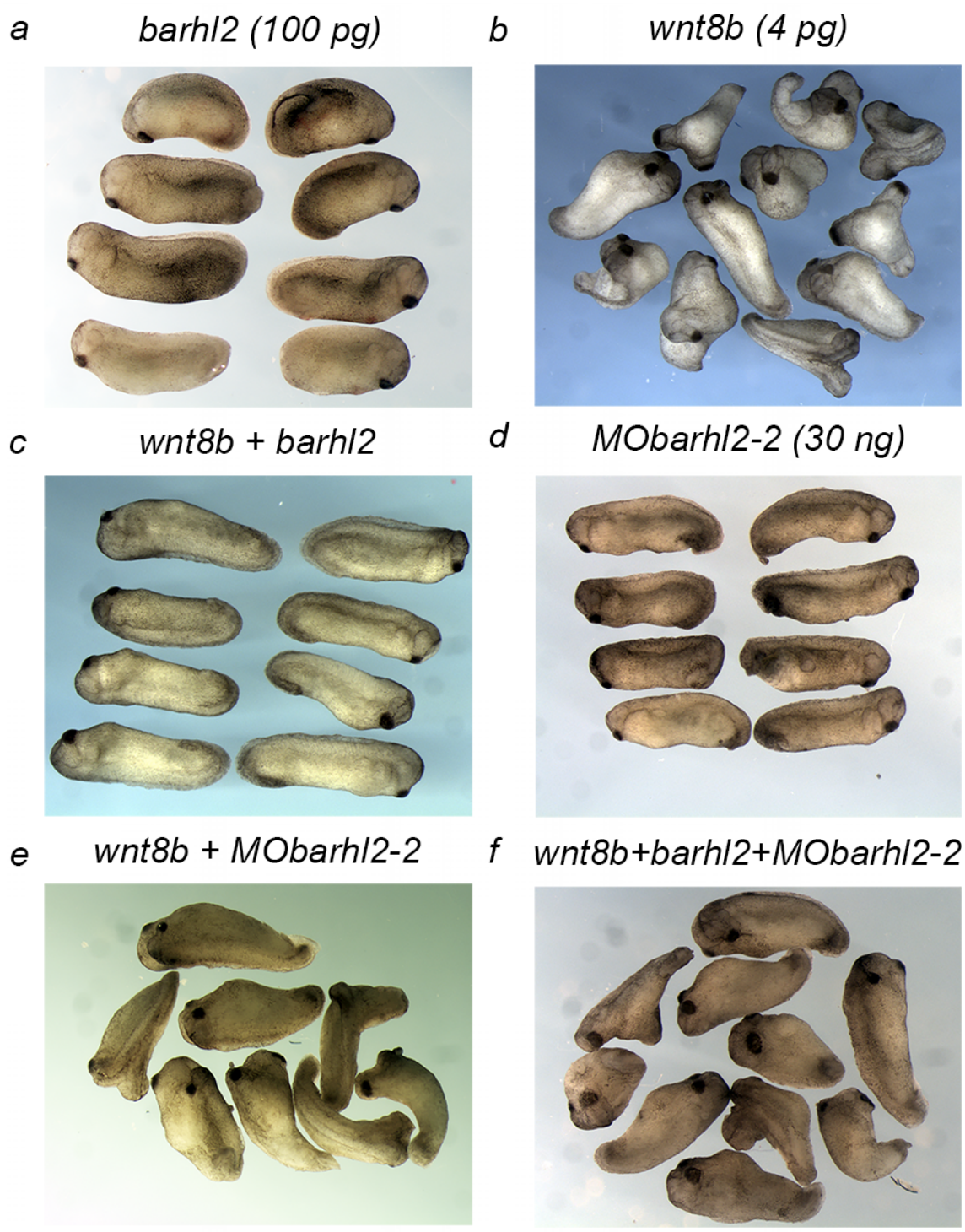

Figure S7: Representative embryos for the experiment described in Fig. 4G. Representative *X. laevis* embryos are shown injected into one ventral blastomere at the 4-cell stage with (a) RNA encoding *barhl2* (100 pg); (b) RNA encoding *wnt8b* (4 pg); (c) *barhl2* (100 pg) and *wnt8b* (4 pg); (d) *MObarhl2* (30 ng); (e) *wnt8b* (4 pg) and *MObarhl2* (30 ng); (f) *barhl2* (100 pg) with *wnt8b* (4 pg) and *MObarhl2* (30 ng).

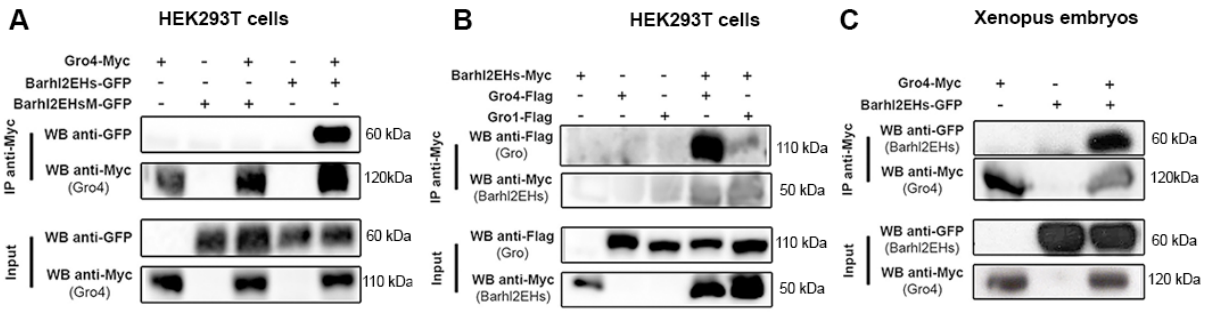

Figure S8: Barhl2EHs interacts preferentially with Gro4. HEK293T cells were co-transfected with vectors (0.5 µg to 2 µg) encoding indicated proteins and embryos were injected with tagged mRNA coding for Gro-Myc or Barhl2EHs-GFP. Co-IP was performed on either cells' or embryos' stage 10 protein extracts using an anti-Myc antibody. Total lysates and the immunoprecipitated complexes were analyzed with WB analysis using antibodies as indicated. (A) In mammalian cells Gro4 interacts with Barhl2EHs but not with Barhl2EHsM that carries mutations in its two EH1 domains. (B) Barhl2EHs co-immunoprecipitates with both Gro4 and Gro1 but exhibits a stronger affinity for Gro4. Transcripts coding for co-repressors Gro1, 2, and 4 proteins are present in blastula embryos and interact with both Tcf and EH1 (Roose et al., 1998; Houston et al., 2002; Owens et al., 2016), and Gro4 is required for Xenopus organizer formation (Roose et al., 1998). We observed that Barhl2EHs co-immunoprecipitated with Gro4 with a higher efficiency then Gro1, arguing that Barhl2EHs interacts preferentially with Gro4. (C) Gro4 interacts with Barhl2EHs in Xenopus embryos.

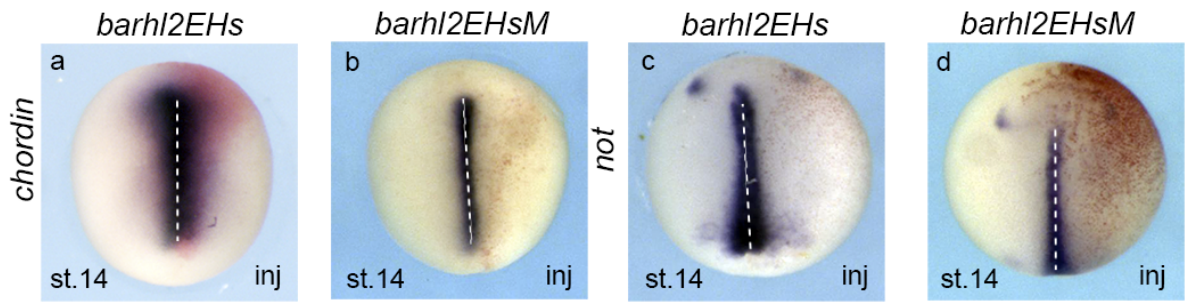

Figure S9: Barhl2EHs induces an increase of the notochord size at stage 14. ISH on stage (st) 14 embryos using (a,b) *chordin* (c,d) or *not*, two markers of the notochord as probes on embryos injected into one dorsal blastomere at the 4-cell stage, together with a tracer (red). Representative embryos injected with (a,c) barhl2EHs or (b,d) barhl2EHsM encoding RNA are shown dorsal view, anterior up. inj: injected side.

Figure S10: Quantification of rescue staining of Figure 6F. ISH using probes against *chd* on stage 10 embryos injected either with RNAs coding for *barhl2*, or with *MOhdac1* separately or together. The top panel corresponds to the injected side. Each embryo was individually analyzed and all analyzed embryos are shown. The control and injected sides were delimited based on tracer. Panels are shown as in supplementary Figure 2. (A) embryos injected with *barhl2fl*; (B) embryos injected with *MOhdac1*; (C) embryos injected with *barhl2fl* and *MOhdac1*.

Figure S10A: Embryos injected with *Xbarhl2fl*.

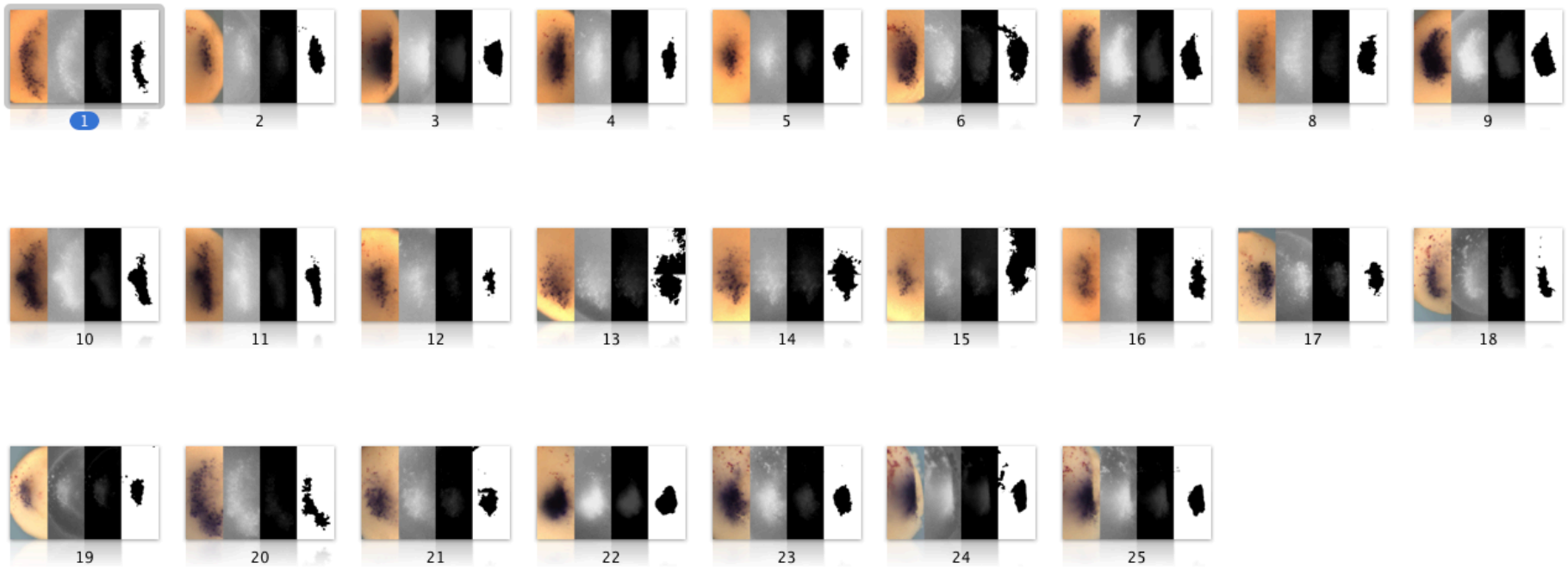

Figure S10B: Embryos injected with *MOhdac1.*

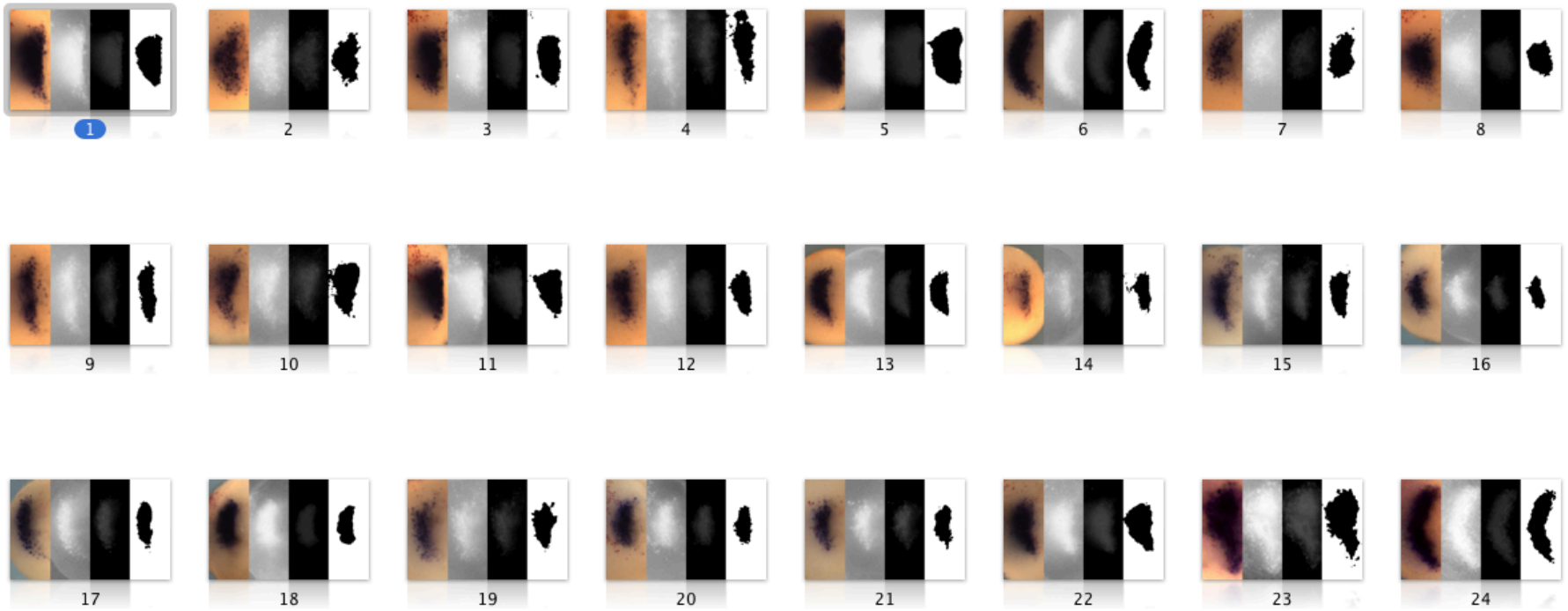

Figure S10C: Embryos injected with *Xbarhl2fl* and *MOhdac1*.

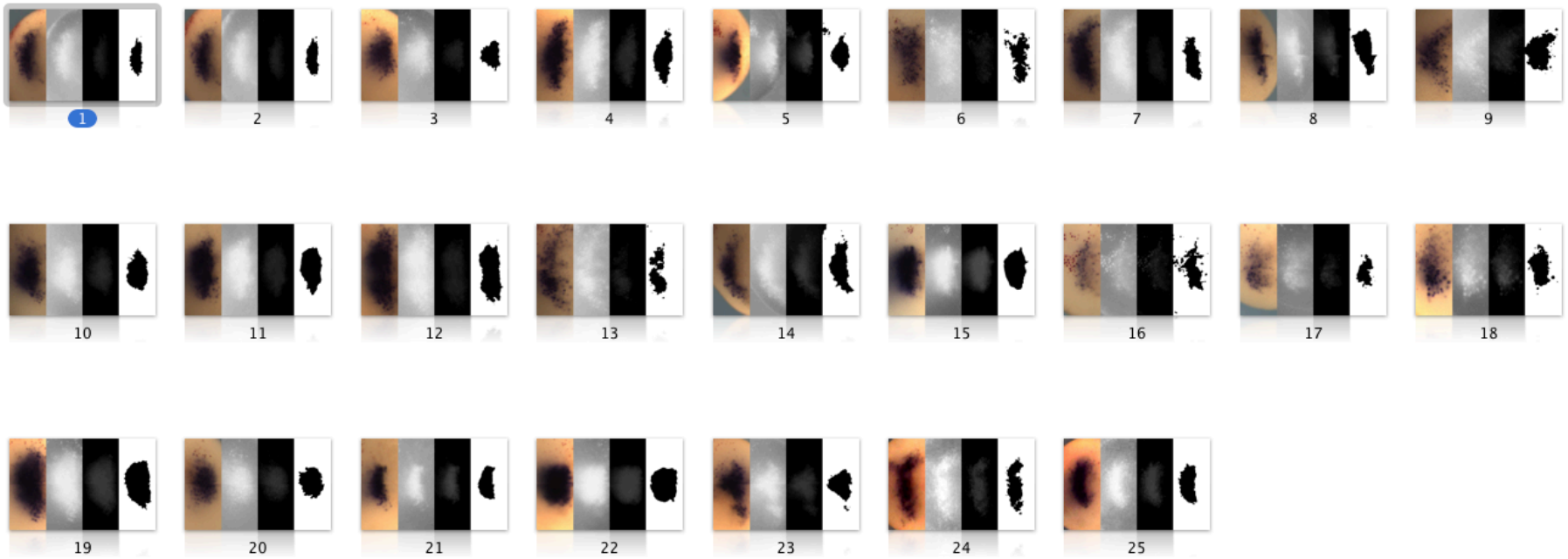

References

Borday, C., Cabochette, P., Parain, K., Mazurier, N., Janssens, S., Tran, H. T., Sekkali, B., Bronchain, O., Vleminckx, K., Locker, M. et al. (2012) 'Antagonistic cross-regulation between Wnt and Hedgehog signalling pathways controls post-embryonic retinal proliferation', *Development* 139(19): 3499-509.

Borday, C., Parain, K., Thi Tran, H., Vleminckx, K., Perron, M. and Monsoro-Burq, A. H. (2018) 'An atlas of Wnt activity during embryogenesis in Xenopus tropicalis', *PLoS One* 13(4): e0193606.

Gamse, J. T. and Sive, H. (2001) 'Early anteroposterior division of the presumptive neurectoderm in Xenopus', *Mech Dev* 104(1-2): 21-36.

Houston, D. W., Kofron, M., Resnik, E., Langland, R., Destree, O., Wylie, C. and Heasman, J. (2002) 'Repression of organizer genes in dorsal and ventral Xenopus cells mediated by maternal XTcf3', *Development* 129(17): 4015-25.

Owens, N. D., Blitz, I. L., Lane, M. A., Patrushev, I., Overton, J. D., Gilchrist, M. J., Cho, K. W. and Khokha, M. K. (2016) 'Measuring Absolute RNA Copy Numbers at High Temporal Resolution Reveals Transcriptome Kinetics in Development', *Cell Rep* 14(3): 632-47.

Roose, J., Molenaar, M., Peterson, J., Hurenkamp, J., Brantjes, H., Moerer, P., van de Wetering, M., Destree, O. and Clevers, H. (1998) 'The Xenopus Wnt effector XTcf-3 interacts with Groucho-related transcriptional repressors', *Nature* 395(6702): 608-12.

Tran, H. T., Sekkali, B., Van Imschoot, G., Janssens, S. and Vleminckx, K. (2010) 'Wnt/beta-catenin signaling is involved in the induction and maintenance of primitive hematopoiesis in the vertebrate embryo', *Proc Natl Acad Sci U S A* 107(37): 16160-5.

Table S1. RT-qPCR primers used in this study.

Gene	Forward	Reverse	Reference
barhl2	TTAGGGATGTCAGGGCTACG	ATGGACGCTGTCCACTAACC	This study
brachyury	ATGGTGGAGGCCAGATTATG	TCATTCTGGTATGCGGTCAC	(Yasuoka et al., 2014)
chd	CATGCTCTTTCGAAGGTCAA	GATCACAAATCACGGTACGC	(Inomata et al., 2013)
ef1	ACACTGCTCACATTGCTTGC	AGAAGCTCTCCACGCACATT	This study
gsc	TGAACAACTGGAAGCACTGG	TTCTGCCTCCTCCACTTTGC	This study
not	CTGCATTTGGCCACCACCTGGC	GATGAGCCACACGGGTGGGTA	(Kofron et al., 2004)
odc	CATGGCATTCTCCCTGAAGT	TGGTCCCAAGGCTAAAGTTG	(Milet et al., 2013)
otx2	CGGGATGGATTTGTTGCA	TTGAACCAGACCTGGACT	(Heasman et al., 2000)
sia1	CTGTCCTACAAGAGACTCTG	TGTTGACTGCAGACTGTTGA	(Heasman et al., 2000)
vent2	CCTCGGTTGAATGGCTTGCT	TGAGACTTGGGCACTGTCTG	(Kofron et al., 2004)
wnt8a	CTGATGCCTTCAGTTCTGTGG	CTACCTGTTTGCATTGCTCGC	(Heasman et al., 2000)

Table S2. Quantitative PCR primers for promoter analysis (ChIP) used in this study.

Gene	Forward	Reverse	Reference
chd	GTGGACCCTGTGGATTATGG	GCTGGAGTCTTGGATTGGAG	This study
ef1	GTCTCGGCCCCTAAATATGA	CAGCTCCCAGCTCTTTTGTC	(Blythe et al., 2009)
gdpah	AATGAGGTGCATGCTGGGTT	GCCAGAGCCCCTCTTACTCT	This study
gsc	AATGACAGCCAACAGCTCAGAGGACA	TCGCAGACTCTCCCTGTAGTTATTCACA	(Blythe et al., 2009)
gsc prom	CCAGAGAAACAAAACAGTCATTCC	GGTGCAATTTCCTTGCTCTC	(Li et al., 2013)
otx2	TTGTGCTCCCTGATCAAACA	ATATCCCACCGACGGATGTA	This study
sia1	GGGACTTTGAAGTCTTGCCA	TCTGATGACACGTGTTTCCC	(Blythe et al., 2009)

Table S3. Primary antibodies used in this study.

Primary antibody	Source	Host	Dilution	Use
c-Myc epitope	SC clone 9E10	Mouse	1:5000	Western Blotting
Flag epitope	Sigma-Aldrich F7425	Rabbit	1:1000	Western Blot
GFP epitope	Abcam ab32146	Rabbit	1:1000	Western Blotting
HA epitope	Roche clone 3F10	Rat	1:500	Western Blotting
H3K9ac	Abcam 4441	Rabbit	2ug/reaction	Chromatin Immunoprecipitation
AM- epitope	Active motif clone 61677	Rabbit	1:1000	Western Blotting

Table S4. Secondary antibodies used in this study.

Secondary antibody	Source	Host	Dilution	Use
HRP anti-mouse IgG	Jackson ImmunoResearch 115-035-003	Goat	1:10000	Western Blotting
HRP anti-rabbit IgG	Jackson ImmunoResearch 111-035-003	Goat	1:10000	Western Blotting
HRP anti-rat IgG	Santa Cruz Biotechnology sc-2006	Goat	1:10000	Western Blotting
HRP anti-rat IgG light chain specific	Jackson ImmunoResearch 112-035-175	Goat	1:10000	Western Blotting